ANALYSIS OF OSCILLATORY FLOW AND HEAT TRANSFER IN AN OSCILLATING HEAT PIPE

A Thesis

presented to

the Faculty of the Graduate School

at the University of Missouri-Columbia

In Partial Fulfillment

of the Requirements for the Degree

Master of Science

by

WEI SHAO

Dr. Yuwen Zhang, Thesis Supervisor

MAY 2010

The undersigned, appointed by the dean of the Graduate School, have examined the thesis entitled

ANALYSIS OF OSCILLATORY FLOW AND HEAT TRANSFER IN AN OSCILLATING HEAT PIPE

presented by Wei Shao,

a candidate for the degree of master of science,

and hereby certify that, in their opinion, it is worthy of acceptance.

Professor Yuwen Zhang

Professor Gary Solbrekken

Professor Ping Yu

ACKNOWLEDGEMENTS

I would like to thank Dr. Zhang for his continued support and guidance throughout the project. I am very grateful for the help he gave me not only on the work but also on the daily life. I would also like to thank the members of my thesis evaluation committee, Dr. Gary Solbrekken and Dr. Ping Yu for taking the time to provide valuable comments and criticism. I would like to thank Pat Frees ad Melanie Gerlach for all their helps on my graduate paperwork.

I would like to thank all my coworkers, Jianhua Zhou, Jing Huang, Lingqi Yang, Tao Jia, Hongbo Kang, Qicheng Chen, Kapil Baheti, Piyasak Damronglerd and Nazia Afrin. It is a really wonderful time to work with them.

I also want to thank my friends Fay Wang, Qian Chen, Weijun Huang, Dongdong Zhang, Yanyan Zhang, Jia You, Dr Changping Yu and Yu Yang here. Thank you, Ye Zhu, my best friend! The time we spend together I will never forget and wish you all have a shining future.

I would like to express my gratitude to my parents, Boli Zhu and Zhongming Shao, who stand by me and give me the courage and strength I need to complete this work. Without all the love and support I have received all these years from my parents, I would never have been able to successfully reach my academic goals.

Thanks to all of you, I was able to accomplish more than I expected and reconsider everything I have done and find out what is the most important thing in my life and I am certain about who I am going to be in the future

TABLE OF CONTENTS

LIST OF FIGURES

LIST OF TABLES

Table Page

NOMENCLATURES

A	area, m^2
C_l	friction coefficient
c_p	specific heat at constant pressure, J/kg•K
c_v	specific heat at constant volume, J/kg•K
d	diameter of the minichannel, m
G_n	constant
h_{lv}	latent heat of vaporization, J/kg
h_e	heating coefficient, J/kg•K
h_c	cooling coefficient, J/kg•K
h_{lsen}	convection heat transfer coefficient, J/kg
k	thermal conductivity, W/m-K
K	curvature, 1/m
L	length, m
L_1	length of thin film in the evaporator section, m
L_2	length of thin film in the condenser section, m
m	mass of vapor plugs, kg
$\dot{m}$	mass flow rate, kg/s
Nu	Nusselt number
p	vapor pressure, Pa
Pr	Prantle number
Re	Reynolds number
R_g	gas constant, J/kg-K
R	radius of the minichannel, m

r	radial coordinate, m
s	axial coordinate in meniscus reion, m
t	time, s
T	temperature, K
v_p	velocity of the liquid plug, m/s
x_p	displacement of the liquid plug, m
x^+	dimensionless coordinates on the liquid plug
Q_{eva}	evaporation heat transfer, W
Q_{con}	condensation heat transfer, W
Q_h	sensible heat transfer into the liquid plug, W
Q_c	sensible heat transfer out of the liquid plug, W
Q_l	latent heat transfer, W
Q_s	sensible heat transfer, W
w	velocity, m/s

Greek symbols

α	thermal diffusivity, m^2/s
γ	ratio of specific heats
δ	liquid film thickness m
Δ	slope of liquid film
Δp_b	pressure loss at bend, Pa
ζ	loss coefficient
θ	contact angle
λ_n	eigen value

μ	dynamic viscosity, N•s/m^2
ξ	dimensionless coordinate where wall temperature varies
ρ	density, kg/m^3
σ	surface tension N/m
τ	shear stress, N/m^2

Subscripts

0	initial condition
a	advancing
c	condenser
cap	capillary
d	disjoining pressure
e	evaporator
i	index of vapor slugs
in	inlet
l	liquid
m	mean
me	meniscus
p	plug
r	receding
sat	saturation
tr	transient
v	vapor
w	wall of the tube

ABSTRACT

An advanced physical and theoretical model of a U-shaped minichannel – a building block of an Oscillating Heat Pipe (OHP) – has been developed step by step.

a) The gravity and pressure loss at the bend are included in the momentum equation of the liquid slug. The sensible heat transfer coefficient between the liquid slug and the minichannel wall are obtained by analytical solution for laminar liquid flow and by empirical correlations for turbulent liquid flow. Besides, the effect of axial step variation of surface temperature is considered by using method of superposition to calculate the sensible heat transfer coefficients between the liquid slug and the minichannel wall in laminar region. The evaporation and condensation heat transfer coefficients are simply assumed. The role of axial variation of surface temperature is mainly on the liquid flow dominated by laminar region and the pressure loss at the bend delays the phase of oscillation.

b) Capillary force and inclination angle are added into the momentum equation of the liquid slug to investigate the surface tension and gravity effects on the oscillatory flow and heat transfer in an OHP with different inner diameters and orientations. The results show that gravity effect hinders the performance of top heat mode OHP while aids the operation of bottom heat mode OHP. Comparisons between the cases with surface tension and without surface tension indicate that the effect of surface tension on the performance of OHP is negligible even for small inner diameter.

c) Film evaporation and condensation models are consistently specified to calculate latent heat transfer happened in the evaporator and condenser. Precise prediction of latent heat transfer due to phase change can be given by current heat transfer model.

CHAPTER 1 INTRODUCTION

1.1 Background

The increased demanding on high performance required by the IT industry has raised thermal design challenges due to both increased heat dissipation from the CPU and higher heat density. Local hot spot heat fluxes within the CPU are exceeding 100W/cm^2 causing the CPU temperature rise, malfunction and failure of CPU without a very effective heat transfer device. While conventional heat sinks or spreaders become severely inadequate at these high levels of heat fluxes, Oscillating (or Pulsating) Heat Pipe (OHP or PHP) shows promise to meet the next generation CPU thermal requirements with a low profile heat sink. The OHP is a new type of two-phase heat transfer devices, invented and patented in 1990's by Akachi [1]. Due to its potential heat transport capability, fast thermal response, simple structure and low cost of construction, the OHP will play a key role in the electronics cooling.

1.2 Mechanism of Oscillating Heat Pipes

Typically, an OHP consists of a plain meandering long tube of capillary dimensions with many U-turns and joined end to end and the evaporator and condenser sections are located at these turns. Compared with the traditional heat pipes, the unique feature of OHP is that the vapor and liquid flow in the same direction, and therefore there is no friction between the liquid and vapor phases. The inner diameter of an OHP should be sufficiently small ranging from 0.1mm to 5 mm so that under operation conditions liquid slugs and vapor plugs can be formed by the surface tension [2]. There is no wick

structure to return condensate liquid from the condenser to the evaporator section; heat is transported from the evaporator section to the condenser section by the oscillation of the working fluid in the axial direction in the tube. When the evaporator section is heated, the vapor pressure at this end increases due to higher temperature and liquid evaporation. At another cooling end of the heat pipe, when the vapor bubbles are cooled, the bubble collapse, the condensing liquid film is formed inside the channel and the pressure in the condenser is lower by the reduced temperature and condensation. This increased pressure in the evaporator and reduced pressure in the condenser results in a pressure difference. This pressure difference pushes the hot vapor and liquid from the evaporator to the condenser and conversely the cold vapor and liquid from the condenser to the evaporator. In this way, an enhanced transient heat transfer process occurs due to the phase-change heat transfer and forced convection.

1.3 Analysis and Modeling of Oscillating Heat Pipes

In the last decade, extensive experimental and theoretical works have been conducted to understand the mechanism of the OHP. Dobson and Harms [3] developed a simple mathematical model to study the behavior of an OHP with an open-end. They simply assumed the heat transfer coefficients between heated pipe wall and the vapor and neglected the effect of surface tension and heat transfer between the liquid and its surroundings. Hosoda et al. [4] investigated the formation of vapor plugs in a meandering closed loop heat transport device (MCL-HTD) with a simplified numerical model neglecting liquid film between the tube wall and the vapor plug and the effect of surface tension. Wong et al. [5] presented a theoretical model of OHP operation based on the Lagrangian approach of slug flow in a serpentine tube. By using a pressure pulse

generated by the local heat input into the vapor bubble, the pressure and velocity variations in the OHP were obtained. The liquid film between the vapor plug and the wall and the effect of surface tension were not included. Zhang and Faghri [6] analyzed thin film evaporation and condensation in the evaporator and condenser sections of an OHP with an open end. The results showed that the heat transfer in an OHP is mainly due to the exchange of sensible heat and phase-change heat transfer is the driving force of the oscillation. Liang and Ma [2] presented a mathematical model describing the oscillation characteristics of slug flow in a capillary tube. It was demonstrated that the internal diameter, vapor plug size, and unit cell numbers determine the oscillation and capillary force, gravitational force, initial pressure distribution of the working fluid significantly affect the frequency and amplitude of oscillating motion in the capillary tube. Shafii et al. [7], based on thin film evaporation and film condensation, established a theoretical model of an OHP and concluded that the surface tension has little effect on the frequency and amplitude of the oscillation motion. Zhang and Faghri [8] investigated liquid-vapor pulsating flow in an OHP with arbitrary number of turns. The results showed that for an OHP with fewer than six turns the amplitude and frequency of oscillation are independent of the number of turns. Kiseev and Zolkin [9] experimentally investigated the effects of acceleration and vibration on the performance of the unlooped OHP and the results indicated that the OHP operates successfully by various acceleration effects. By increasing the acceleration from -6g to +12g the evaporator temperature was increased by 30%. Ma et al. [10] developed a mathematical model predicting the fluid motion and temperature drop in an OHP. The numerical results indicate that the oscillating motions occurring in the OHP significantly enhances the heat transfer in the OHP. Experimental

results indicated that there exists an onset temperature difference for the excitation of oscillating motions in an OHP. In order to fully discover the mechanisms of OHP operation and performance, the microfilm and thick-film evaporation and condensation need detailed investigation. Khrustalev and Faghri [11] developed a physical and mathematical model of the evaporating thick liquid film attached to the liquid-vapor meniscus in a circular micropore. The numerical results obtained for water demonstrate that formation of extended thick liquid films in micropores can take place due to high-velocity vapor flow under high rates of vaporization. Begg et al. [12] followed the same trend and established a model of annular film condensation in a miniature tube. The model predicts the shape of the liquid-vapor interface along the condenser and the length of the two-phase flow region. Observations from a flow visualization experiment of water vapor condensing in a horizontal glass tube confirm the existence and qualitative features of annular film condensation leading to the complete condensation phenomenon in small diameter($d<3.5$mm) circular tubes.

1.4 Thesis Objectives

In spite of significant efforts in the last decade, there are still unresolved issues affecting OHP performance. A typical simplifying assumption in many of the mathematical models is to neglect the pressure loss at each bend in the pipe. None of the existing models considered the effects of axial variation of the surface temperature of the tube whose role is mainly on the sensible heat transfer. Conflicting conclusions have been drawn as to whether higher or lower values of surface tension improve OHP performance. The evaporation and condensation heat transfer coefficients are simply assumed in most works which fails to predict the latent heat transfer due to phase change precisely.

The objective of this study is to develop an analytical model for predicting the oscillation motion and heat transfer in an OHP. Detailed numerical simulation is carried out to investigate the effects of pressure loss at the bend, axial variation of surface temperature, surface tension, orientation and thin film evaporation and condensation on the oscillatory flow and heat transfer performance.

1.4.1 Pressure Loss at Bends and Axial Variation of the Wall Temperature

The gravity and pressure loss at the bend are included in the momentum equation of the liquid slug. The sensible heat transfer coefficient between the liquid slug and the minichannel wall are obtained by analytical solution for laminar liquid flow and by empirical correlations for turbulent liquid flow. Besides, the effect of axial variation of surface temperature is considered by using method of superposition to calculate the sensible heat transfer coefficients between the liquid slug and the minichannel wall in laminar region. The evaporation and condensation heat transfer coefficients are simply assumed. The role of axial variation of surface temperature is mainly on the liquid flow dominated by laminar region and the pressure loss at the bend delays the phase of oscillation.

1.4.2 Surface Tension and Orientation

Capillary force and inclination angle are added into the momentum equation of the liquid slug to investigate the surface tension and gravity effects on the oscillatory flow and heat transfer in an OHP with different inner diameters and orientations. The results show that gravity effect hinders the performance of top heat mode OHP while aids the operation of bottom heat mode OHP. Comparisons between the cases with surface tension and without surface tension indicate that the effect of surface tension on the performance of OHP is negligible even for small inner diameter.

1.4.3 Thin Film Evaporation and Condensation

Since evaporation and condensation over the thin liquid film are the driving forces of the oscillation, precise calculation of phase change is desirable. Thin film and thick-film evaporation and thin film condensation models are consistently specified to calculate latent heat transfer happened in the evaporator and condenser. The latent heat transfer due to phase change can be predicted more accurately by current heat transfer model.

CHAPTER 2 PRESSURE LOSS AT BENDS AND AXIAL VARIATION OF SURFACE TEMPERATURE

2.1 Physical Model

2.1.1 Problem Description

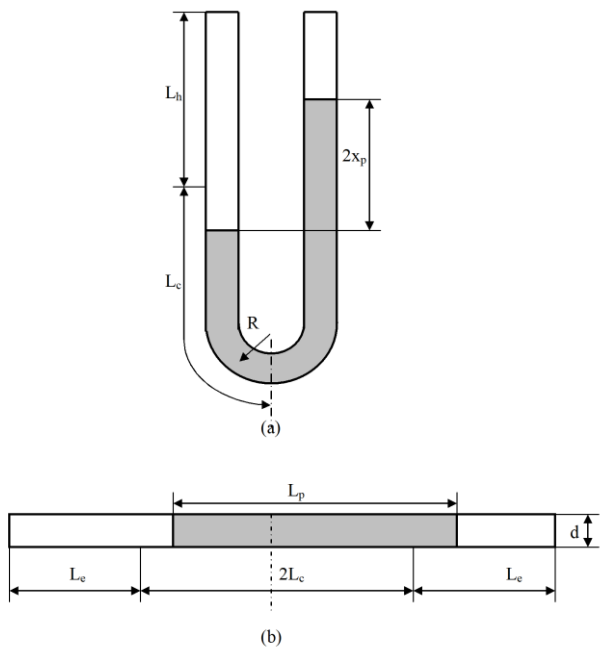

Figure 1 Physical model

Figure 1 shows the physical model of a U-shaped minichannel (see Fig. 1(a)) with its two ends sealed. It is considered as the building block of an OHP. The U-shaped minichannel is treated as a straight tube (see Fig. 1(b)) with the pressure loss at the bend considered. The length of each evaporator section, which is located at the two ends of the pipe, is L_e and evaporator temperature is maintained at T_e. The condenser section is located between two evaporation sections with a length of L_c. The temperature of condenser section is maintained at T_c. The length of the liquid slug is L_p, which depends

on the filling ratio. The density of vapor is only around 0.1 percent of the liquid density at the saturated state and the difference between the speed of condensation and evaporation will not change the length of liquid slug. The displacement of the liquid slug is represented by x_p. When the liquid slug is exactly in the middle of the U-shaped miniature channel, x_p is zero. When the liquid slug shifts to the right side, x_p is positive; when it moves to the left side x_p is negative.

If the initial value of displacement, x_{p0} is positive (see Fig.1 (a)), part of the vapor plug in the left-side is in contact with the condenser section, and condensation in the left part will cause the pressure of the left vapor plug p_{v1} to decrease. The pressure difference between the two vapor plugs causes the liquid slug moving to the left direction. Evaporation from the thin liquid film left behind on the right part of the channel cause the pressure of the right vapor plug p_{v2} to increase and the pressure difference between the two ends of the liquid slug further increases. When the displacement x_p becomes zero, there is neither evaporation nor condensation in two vapor plugs, but the liquid slug keeps moving due to its inertia. When the liquid moves to the left side ($x_p < 0$), the pressure difference changes its sign. The oscillation of the liquid slug can be sustained by alternative evaporation and condensation in the two vapor plugs.

The following assumptions are made in order to model heat transfer and fluid flow in the heat pipe:

(1) The liquid is incompressible and the vapor is saturated and behaves as an ideal gas with no temperature gradient in the vapor region.

(2) Evaporative and condensation heat transfer coefficients are assumed to be constants.

(3) Heat conduction in the liquid slug is assumed to be one-dimensional in the axial direction and exchange of heat between the liquid and wall is considered by a convective heat transfer coefficient.

(4) The U-shaped minichannel is assumed to be a straight pipe and the effect of pressure loss at the bend is considered using an empirical correlation.

2.1.2 Governing Equations for Oscillatory Flow

The momentum equation for the liquid slug is:

$$AL_p\rho_l \frac{d^2x_p}{dt^2} = \left[\left(p_{v1} - p_{v2}\right) - \Delta p_b\right]A - 2\rho_l gAx_p - \pi dL_p\tau_p \tag{1}$$

where $A = \pi d^2/4$ is cross-sectional area, the pressure loss at the bend can be found from Kay et al [13]:

$$\Delta p_b = \begin{cases} \zeta\rho_l \dfrac{v_p^{\,2}}{2} & v_p > 0 \\ -\zeta\rho_l \dfrac{v_p^{\,2}}{2} & v_p < 0 \end{cases}, \tag{2}$$

where ζ is the pressure loss coefficient,

and $\tau_p = c_l\rho v^2/2$ is the shear stress， where the friction coefficient c_l can be found in Gnielinski [14]

$$c_l = \begin{cases} 16/\mathrm{Re} & \mathrm{Re} \le 2200 \\ 0.078\,\mathrm{Re}^{-0.2} & \mathrm{Re} > 2200 \end{cases} \tag{3}$$

The effect of gravity on the motion of the liquid slug has been included in the momentum equation.

Using the first law of thermodynamics to each plug, the energy equations of the two vapor plugs are:

$$\frac{d(m_{v1}c_vT_{v1})}{dt} = c_pT_{v1}\frac{dm_{v1}}{dt} - p_{v1}\frac{\pi}{4}d^2\frac{dx_p}{dt} \tag{4}$$

$$\frac{d(m_{v2}c_vT_{v2})}{dt} = c_pT_{v2}\frac{dm_{v2}}{dt} + p_{v2}\frac{\pi}{4}d^2\frac{dx_p}{dt} \tag{5}$$

Rearranging equations (4) and (5) one obtains:

$$m_{v1}c_v\frac{dT_{v1}}{dt} = R_gT_{v1}\frac{dm_{v1}}{dt} - p_{v1}\frac{\pi}{4}d^2\frac{dx_p}{dt} \tag{6}$$

$$m_{v2}c_v\frac{dT_{v2}}{dt} = R_gT_{v2}\frac{dm_{v2}}{dt} + p_{v2}\frac{\pi}{4}d^2\frac{dx_p}{dt} \tag{7}$$

The vapor plugs behave as an ideal gas, i.e.,

$$p_{v1}(L_e + x_p)\frac{\pi}{4}d^2 = m_{v1}R_gT_{v1} \tag{8}$$

$$p_{v2}(L_e - x_p)\frac{\pi}{4}d^2 = m_{v2}R_gT_{v2} \tag{9}$$

Differentiating eqs. (8) and (9) with respect to time yields:

$$\frac{\pi}{4}d^2\frac{dp_{v1}}{dt}(L_e+x_p)+p_{v1}\frac{\pi}{4}d^2\frac{dx_p}{dt}=m_{v1}R_g\frac{dT_{v1}}{dt}+RT_{v1}\frac{dm_{v1}}{dt} \tag{10}$$

$$\frac{\pi}{4}d^2\frac{dp_{v2}}{dt}(L_e-x_p)-p_{v2}\frac{\pi}{4}d^2\frac{dx_p}{dt}=m_{v2}R_g\frac{dT_{v2}}{dt}+RT_{v2}\frac{dm_{v2}}{dt} \tag{11}$$

Substituting eqs. (6) and (7) into eqs. (10) and (11) respectively to obtain:

$$R_gT_{v1}\frac{dm_{v1}}{dt}=\frac{\pi}{4}d^2\frac{c_v}{c_p}\frac{dp_{v1}}{dt}(L_e+x_p)+p_{v1}\frac{\pi}{4}d^2\frac{dx_p}{dt} \tag{12}$$

$$R_gT_{v2}\frac{dm_{v2}}{dt}=\frac{\pi}{4}d^2\frac{c_v}{c_p}\frac{dp_{v2}}{dt}(L_e-x_p)-p_{v2}\frac{\pi}{4}d^2\frac{dx_p}{dt} \tag{13}$$

Substituting eqs. (8) and (9) into eqs. (12) and (13) respectively to obtain:

$$\frac{1}{m_{v1}}\frac{dm_{v1}}{dt}=\frac{1}{\gamma}\frac{1}{p_{v1}}\frac{dp_{v1}}{dt}+\frac{1}{L_e+x_p}\frac{dx_p}{dt} \tag{14}$$

$$\frac{1}{m_{v2}}\frac{dm_{v2}}{dt}=\frac{1}{\gamma}\frac{1}{p_{v2}}\frac{dp_{v2}}{dt}-\frac{1}{L_e-x_p}\frac{dx_p}{dt} \tag{15}$$

where $\gamma=c_p/c_v$ is the ratio of specific heats of the vapor.

Integrating eqs. (14) and (15), the masses of vapor plugs are obtained as:

$$m_{v1}=C_1p_{v1}^{\frac{1}{\gamma}}(L_e+x_p) \tag{16}$$

$$m_{v2}=C_2p_{v2}^{\frac{1}{\gamma}}(L_e-x_p) \tag{17}$$

where C_1 and C_2 are integral constants. Since the structure of the U-shaped channel is symmetric, the two integral constants are the same, i.e., $C_1 = C_2 = C.$ Substituting eqs. (16) and (17) into eqs. (8) and (9), one obtains the temperatures of both vapor plugs:

$$T_{v1} = \frac{\pi d^2}{4CR_g} p_{v1}^{\frac{(\gamma-1)}{\gamma}} \tag{18}$$

$$T_{v2} = \frac{\pi d^2}{4CR_g} p_{v2}^{\frac{(\gamma-1)}{\gamma}} \tag{19}$$

The integral constant can be determined by choosing a reference state that the displacement of liquid slug is x_{p0} and pressures and temperatures of both vapor plugs are T_0, p_0, respectively. It follows from eqs. (18) and (19) that

$$C_1 = C_2 = C = \frac{\pi d^2}{4R_g T_0} p_0^{\frac{(\gamma-1)}{\gamma}} \tag{20}$$

Combining the above equations, the masses and temperatures of two vapor plugs are obtained:

$$m_{v1} = \frac{\pi d^2 p_0}{4R_g T_0} \left(\frac{p_{v1}}{p_0} \right)^{\frac{1}{\gamma}} (L_e + x_p) \tag{21}$$

$$m_{v2} = \frac{\pi d^2 p_0}{4R_g T_0} \left(\frac{p_{v2}}{p_0} \right)^{\frac{1}{\gamma}} (L_e - x_p) \tag{22}$$

$$T_{v1} = T_0 \left(\frac{p_{v1}}{p_0} \right)^{\frac{(\gamma-1)}{\gamma}} \tag{23}$$

$$T_{v2} = T_0 \left(\frac{p_{v2}}{p_0} \right)^{\frac{(\gamma-1)}{\gamma}} \tag{24}$$

The effects of evaporation and condensation on variation of the masses of the vapor plugs can be calculated as following,

$$\frac{dm_{v1}}{dt} = \begin{cases} -Q_{cond} / h'_{lv,c}, & x_p > 0 \\ Q_{evp} / h'_{lv,e}, & x_p < 0 \end{cases} \tag{25}$$

$$\frac{dm_{v2}}{dt} = \begin{cases} Q_{evp} / h'_{lv,e}, & x_p > 0 \\ -Q_{cond} / h'_{lv,c} & x_p < 0 \end{cases} \tag{26}$$

where $h'_{lv,c} = h_{lv,c} + 0.68 c_{pl} \left(T_{vi} - T_c \right)$, $h'_{lv,e} = h_{lv,e} + 0.68 c_{pl} \left(T_{vi} - T_e \right)$

The initial condition of the U-shaped minichannel in this study is chosen to be identical to the reference state of this system, i.e.,

$$x_p = x_{p0,} \ t = 0 \tag{27}$$

$$p_{v1} = p_{v2} = p_0, \ t = 0 \tag{28}$$

$$T_{v1} = T_{v2} = T_0, \ t = 0 \tag{29}$$

$$m_{v1} = \frac{\pi d^2 p_0}{4 R_g T_0} (L_e + x_{p0}) \tag{30}$$

$$m_{v2} = \frac{\pi d^2 p_0}{4 R_g T_0} (L_e - x_{p0}) \tag{31}$$

2.1.3 Heat Transfer

Heat transfer in an OHP is defined as the total heat transferred from the heating sections to the cooling sections that consists of two parts: one is the latent heat transfer due to evaporation and condensation of the working fluid, and another part is sensible heat transfer due to heat transfer between the minichannel wall and liquid slugs in the form of single-phase heat transfer.

2.1.3.1 Latent Heat Transfer

The evaporation and condensation heat transfer in the left and right vapor plugs is related to the mass flux due to evaporation and condensation:

$$Q_{in,v1} = \frac{dm_{evp,v1}}{dt} h'_{lv,e} \tag{32}$$

$$Q_{out,v1} = \frac{dm_{con,v1}}{dt} h'_{lv,c} \tag{33}$$

$$Q_{in,v2} = \frac{dm_{evp,v2}}{dt} h'_{lv,e} \tag{34}$$

$$Q_{out,v2} = \frac{dm_{con,v2}}{dt} h'_{lv,c} \tag{35}$$

2.1.3.2 Sensible Heat Transfer

Since the liquid slug is assumed to be incompressible, the entire liquid slug oscillates with the same velocity υ_p. The temperature distribution in the liquid slug can be obtained by solving the energy equation for a liquid slug in a coordinate system that is moving with the liquid slug:

$$\frac{1}{\alpha_l}\frac{dT_l}{dt} = \frac{d^2T_l}{dx_l^{\,2}} - \frac{h_{lsen}\pi d}{k_l A}\left(T_l - T_w\right) \tag{36}$$

where the thermophysical properties of the liquid slug is based on the mean temperature of the liquid slug. Equation (36) is subject to the following initial and boundary conditions

$$T = T_0,\ t = 0,\ 0 < x_l < L_p \tag{37}$$

$$T = T_{\upsilon 1},\ x_l = 0 \tag{38}$$

$$T = T_{\upsilon 2},\ x_l = L_p \tag{39}$$

The wall temperature of the tube can be either T_e or T_c, depending on the displacement of the liquid slug, i.e.,

When $x_p > 0$,

$$T_w = \begin{cases} T_c, & 0 < x_l < L_p - x_p \\ T_e, & L_p - x_p < x_l < L_p \end{cases} \tag{40}$$

When $x_p < 0$,

$$T_w = \begin{cases} T_e, & 0 < x_l < |x_p| \\ T_c, & |x_p| < x_l < L_p \end{cases} \tag{41}$$

Since the Reynolds number of the liquid slug varies in a wide range that covers laminar, transition and turbulent flow, the heat transfer coefficient h of the liquid slug varies periodically. For laminar regime, ($\mathrm{Re} = \dfrac{\rho_l v_p d}{\mu_l} < 2200$), the convective heat transfer problem is considered to be thermally developing Hagen-Poiseuille flow problem. With the effect of axial step variation of surface temperature considered, the Nusselt number is obtained using method of superposition Rohsenow et al. [15]:

$$\mathrm{Nu}(x) = \begin{cases} \dfrac{\sum_{n=0}^{\infty} G_n \exp(-\lambda_n^2 x^+)}{2\sum_{n=0}^{\infty}\left(\dfrac{G_n}{\lambda_n^2}\right)\exp(-\lambda_n^2 x^+)}, & 0 < x^+ < \xi \\ \dfrac{\sum_{n=0}^{\infty} G_n \exp(-\lambda_n^2 x^+)\Delta T_{l,\mathrm{I}} + \sum_{n=0}^{\infty} G_n \exp\left[-\lambda_n^2\left(x^+ - \xi\right)\right]\Delta T_{l,\mathrm{II}}}{2\sum_{n=0}^{\infty}\left(\dfrac{G_n}{\lambda_n^2}\right)\exp(-\lambda_n^2 x^+)\Delta T_{l,\mathrm{I}} + 2\sum_{n=0}^{\infty}\left(\dfrac{G_n}{\lambda_n^2}\right)\exp\left[-\lambda_n^2 (x^+ - \xi)\right]\Delta T_{l,\mathrm{II}}}, & \xi < x^+ < L_p^+ \end{cases} \tag{42}$$

where $L_p^+ = 2L_p/(d\,\mathrm{Re}\,\mathrm{Pr})$ is dimensionless length of the liquid slug, the eigenvalues λ_n and the constant G_n can be found in Rohsenow et al. [15]. The parameters and variables used in eq. (42) are different for different displacements and direction of liquid flow (see Table 1). In contrast to the existing models in the literature that assumed constant heat transfer coefficient, variation of Nusselt number along the length of the liquid slug is taken into consideration.

Table 1 Parameters and variables for laminar sensible heat transfer, eq. (42)

	x^+	ξ	$\Delta T_{l,\mathrm{I}}$	$\Delta T_{l,\mathrm{II}}$
$x_p > 0, v_p > 0$	$\frac{2(x_l/d)}{\mathrm{Re}\,\mathrm{Pr}}$	$\frac{2[(L_p - x_p)/d]}{\mathrm{Re}\,\mathrm{Pr}}$	$T_c - T_{v1}$	$T_e - T_c$
$x_p > 0, v_p < 0$	$\frac{2[(L_p - x_l)/d]}{\mathrm{Re}\,\mathrm{Pr}}$	$\frac{2(x_p/d)}{\mathrm{Re}\,\mathrm{Pr}}$	$T_e - T_{v2}$	$T_c - T_e$
$x_p < 0, v_p > 0$	$\frac{2(x_l/d)}{\mathrm{Re}\,\mathrm{Pr}}$	$\frac{2(-x_p/d)}{\mathrm{Re}\,\mathrm{Pr}}$	$T_e - T_{v1}$	$T_c - T_e$
$x_p < 0, v_p < 0$	$\frac{2[(L_p - x_l)/d]}{\mathrm{Re}\,\mathrm{Pr}}$	$\frac{2[(L_p + x_p)/d]}{\mathrm{Re}\,\mathrm{Pr}}$	$T_c - T_{v2}$	$T_e - T_c$

In the transition and turbulent regions, the following empirical correlations are used Gnielinski [14]:

$$Nu = 0.012(|\mathrm{Re}|^{0.87} - 280)\,\mathrm{Pr}^{0.4}\left(\frac{\mathrm{Pr}_m}{\mathrm{Pr}_w}\right)^{0.11}\left[1+\left(\frac{d}{L_p}\right)^{\frac{2}{3}}\right],\quad 2200 < \mathrm{Re} < 10000 \tag{43}$$

$$Nu = 0.0236|\mathrm{Re}|^{0.8}\,\mathrm{Pr}^{0.43}\left(\frac{\mathrm{Pr}_m}{\mathrm{Pr}_w}\right)^{0.25},\ |\mathrm{Re}| > 10000 \tag{44}$$

The sensible heat transfer into and out from the liquid slug can be obtained by integrating the heat transfer over the length of the liquid slug, i.e.

$$Q_h = \begin{cases} \int_{L_p - x_p}^{L_p} \pi d h_e (T_e - T_l) dx_l,\ x_p > 0 \\ \int_0^{|x_p|} \pi d h_e (T_e - T_l) dx_l,\ x_p < 0 \end{cases} \tag{45}$$

$$Q_c = \begin{cases} \int_0^{x_p} \pi d h_c (T_l - T_c) dx_l, \ x_p > 0 \\ \int_{|x_p|}^{L_p} \pi d h_c (T_l - T_c) dx_l, \ x_p < 0 \end{cases} \tag{46}$$

where the sensible heat transfer coefficient can be obtained from $h = Nuk_l / d$.

2.2 Numerical Procedure

The governing equations in the above physical model can be solved numerically. An explicit finite difference scheme is employed to solve the governing equations of the vapor plugs and the liquid slug. An implicit scheme with uniform grid [16] is employed to solve transient heat transfer in the liquid slug. The total number of grids chosen for the liquid slug is 300 and doubling the number of grids does not the change the results. The results of each time-step can be obtained by the numerical procedure outlined below:

1) Assume the temperatures of the two vapor plugs T_{v1} and T_{v2}, and calculate thermal and physical properties of liquid according to T_l

2) Solve for vapor pressures, p_{v1} and p_{v2}, from eqs. (21) and (22).

3) Solve for x_p from eqs. (1) and (3).

4) Obtain the new masses of the two vapor plugs m_{v1} and m_{v2}, by accounting for the change of vapor masses from eqs. (25) and (26).

5) Calculate the pressure of the two vapor plugs, p_{v1} and p_{v2}, from eqs. (21) and (22).

6) Solve for T_{v1} and T_{v2} from eqs. (23) and (24).

7) Compare T_{v1} and T_{v2} obtained in Step 6 with assumed values in step 1. If the differences meet the small tolerance, then go to the step 8; otherwise, the above procedure is repeated until a converged solution is obtained.

8) Obtain heat transfer coefficient through eqs. (42) to (44).

9) Solve for liquid temperature distribution from eq. (36) and calculate Q_h and Q_c with eqs. (45) and (46).

10) Use eqs. (32) - (35) to calculate Q_l

After the time-step independent test, it was found that the time-step independent solution of the problem can be obtained when time-step is $\Delta t = 1\times10^{-4}$, which is used in all numerical simulations.

2.3 Results and Discussions

The parameters of the miniature channel are: L_e = 0.1 m, L_c = 0.2 m, L_p = 0.2, d = 0.00334m, T_e = 120 °C, T_c =20 °C. The initial pressures of the vapor plugs are P_{v0} =31164.64 Pa and the initial temperature of the vapor plug is T_{v0} = 70 °C. The heat transfer coefficients at the heating and cooling sections are $h_e = h_c$ = 200 W/m^2-K. Unless stated otherwise, the above conditions remain the same for each case.

2.3.1 The effect of pressure loss at the bend

Simulations are then carried out for the cases with pressure loss at the bend and the results are compared with the case without pressure loss at the bend in Figs. 2 through 7. The radius of the bend (see Fig. 1(a)) is 5.83 mm, which results in a pressure loss coefficient $\zeta = 0.31$. Figure 2 (a) shows the effect of the pressure loss at the bend on the

oscillation of liquid slug during the first second. It can be seen that the pressure loss at the bend does not have significant effects on the amplitudes and angular frequencies of the oscillation at the first second. The effect of the pressure loss at the bend on the oscillation of liquid slug after steady oscillation is established is shown in Fig. 2 (b). It can be seen that the pressure loss at the bend delays the phase of oscillation. The phase of oscillation without pressure loss at the bend is half period ahead of that for pressure loss at the bend while the frequency of oscillation is not affected by the pressure loss at bend. In addition, the pressure loss at the bend also causes very insignificant decrease of the amplitude of the liquid slug oscillation.

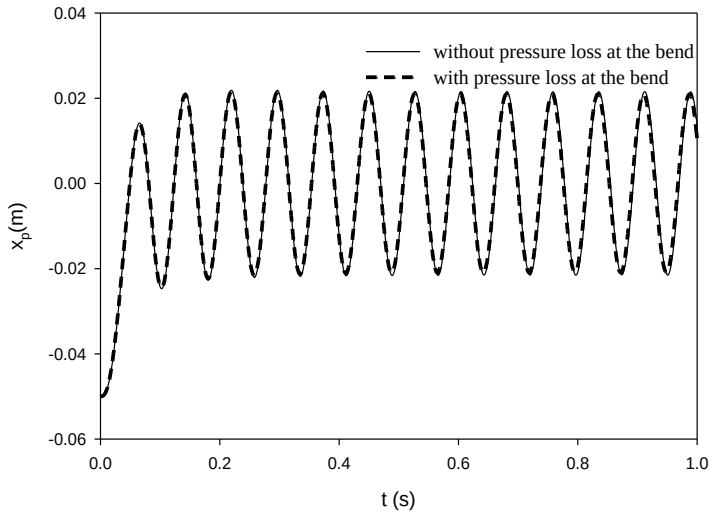

(a) Startup stage

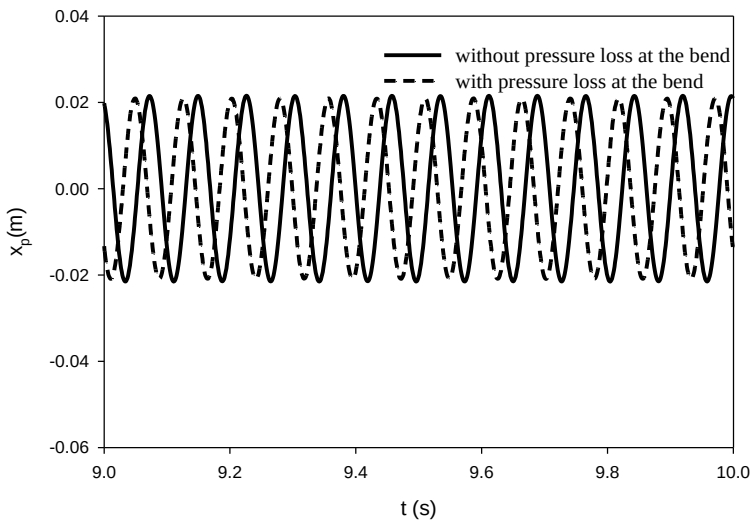

(b) Steady oscillation

Figure 2 Effect of pressure loss in bend on liquid slug displacement

Figure 3 shows the transient response of average mean temperature of liquid slug for the cases with and without pressure loss at the bend. It can be seen that the steady oscillations for both cases are achieved almost at the same time. Moreover, the average mean temperatures of liquid slug for the cases with and without pressure loss at the bend are almost the same. Therefore, the pressure loss at the bend has no effect on the liquid slug mean temperatures.

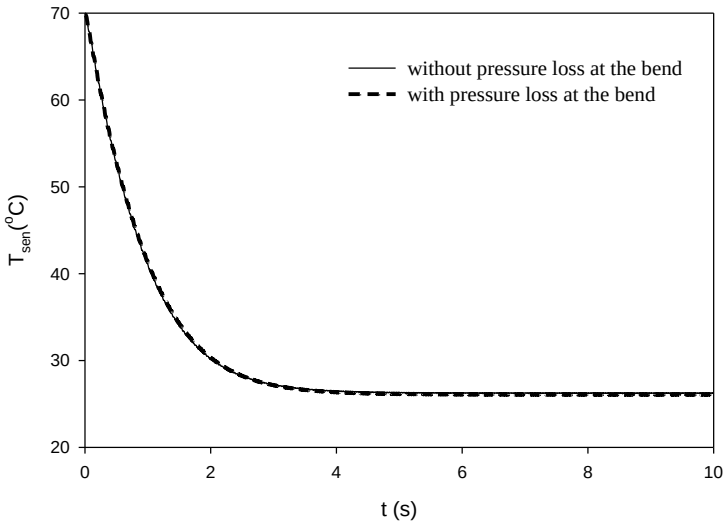

Figure 3 Effect of pressure loss in bend on the average mean temperature of liquid slug

Figure 4 and 5 show the variations of vapor temperature and pressure for the cases with and without pressure loss at the bend. Similar trend as the displacement of liquid slug can be observed from these two figures. The oscillation of vapor temperature and pressure has a half period delay with pressure loss at the bend. In addition, the pressure loss at the bend also slightly decreases the amplitudes of the oscillation of vapor temperature and pressure although the frequency remains the same.

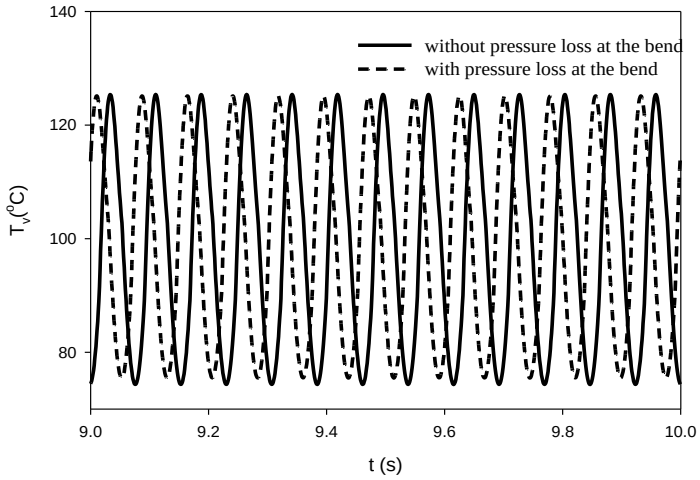

(a) Left vapor plug

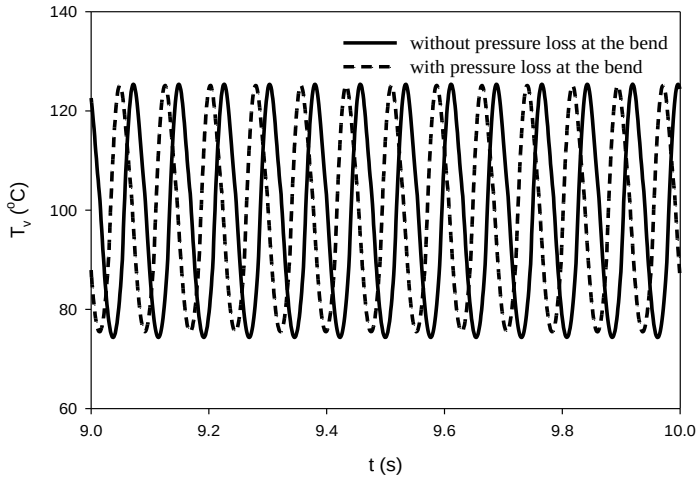

(b) Right vapor plug

Figure 4 Effect of pressure loss in bend on the vapor temperature

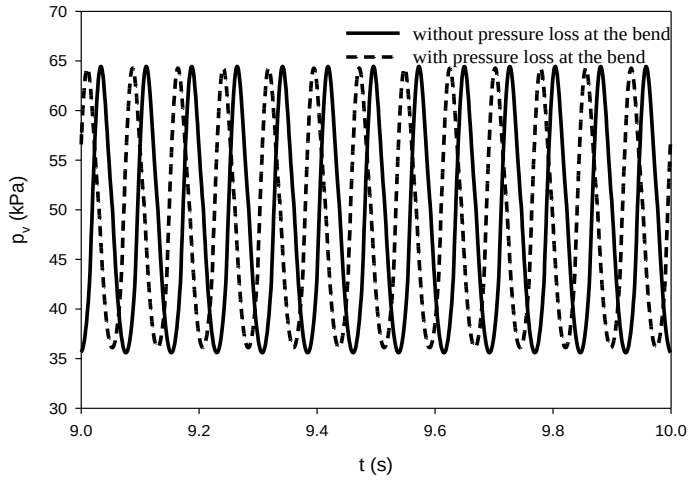

(a) Left vapor plug

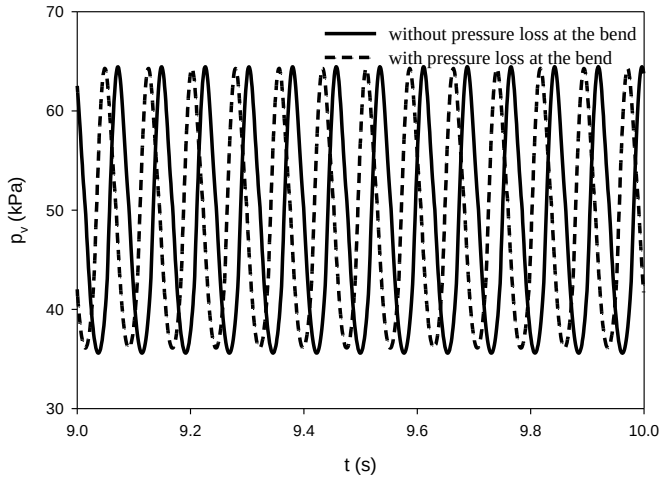

(b) Right vapor plug

Figure 5 Effect of pressure loss in bend on the vapor pressures

The effect of pressure loss at bend on the latent heat transfer is shown in Fig. 6, which has a similar trend of the displacement of liquid slug oscillation. There is only a phase delay after including pressure loss at the bend and a little decrease on the amplitude of the latent heat transfer although the frequency remains the same. Figure 7 shows the effect of pressure loss at the bend on the sensible heat transferred into and out of the system. The sensible heat transfer also demonstrated the similar trend: there is only a phase delay after

including pressure loss at the bend and a little decrease of the sensible heat transfer and the frequency remains unchanged. The system without pressure loss at the bend has higher average heat transfer rate than the system with pressure loss.

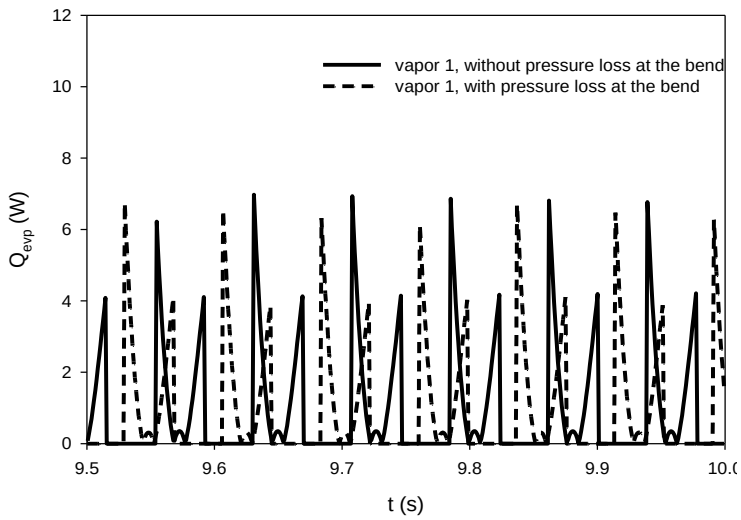

(a) Evaporation

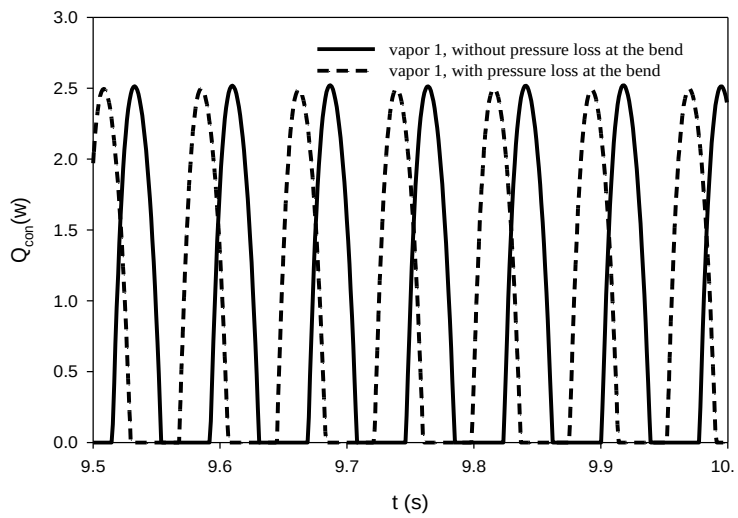

(b) Condensation

Figure 6 Effect of pressure loss in bend on evaporation and condensation of the left plug

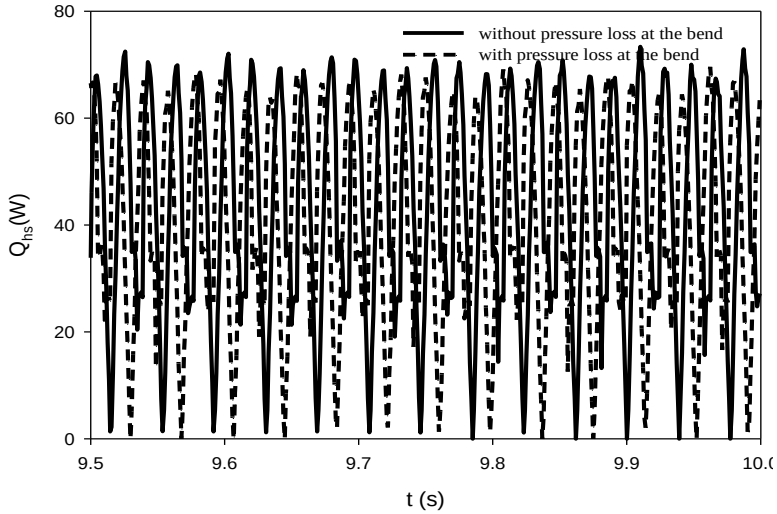

(a) Sensible heat transferred into the liquid slug

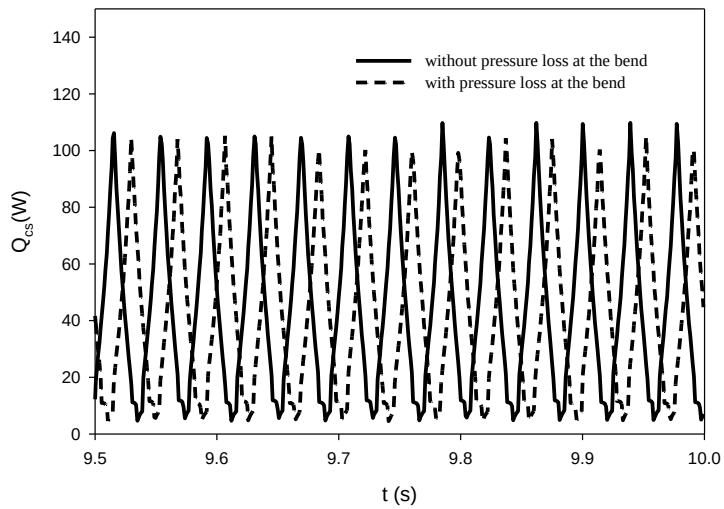

(b) Sensible heat transferred out of the liquid slug

Figure 7 Effect of pressure loss in bend on sensible heat transfer

2.3.2 The effect of axial step variation of wall temperature

Figure 8 shows the effect of different Nusselt number on the mean temperature of the liquid slug. As the heat transfer coefficient between the liquid slug and the wall is not treated as uniform, the calculation of heat transfer coefficient is more accurate than the method used in the existing works. For the same heating and cooling temperatures, the

result from the variable Nusselt number model has a smoother transition from startup to steady oscillating motion. For variable Nu model, the steady-state is reached a little slower than the constant Nu model. The final temperature of the liquid slug for variable Nu model is slightly higher than that for constant Nu model because the heat transfer coefficients for segment I in heating and cooling section are higher under the variable Nu model. The current model includes the effect of thermal entry length on heat transfer and the axial temperature variation in laminar regime.

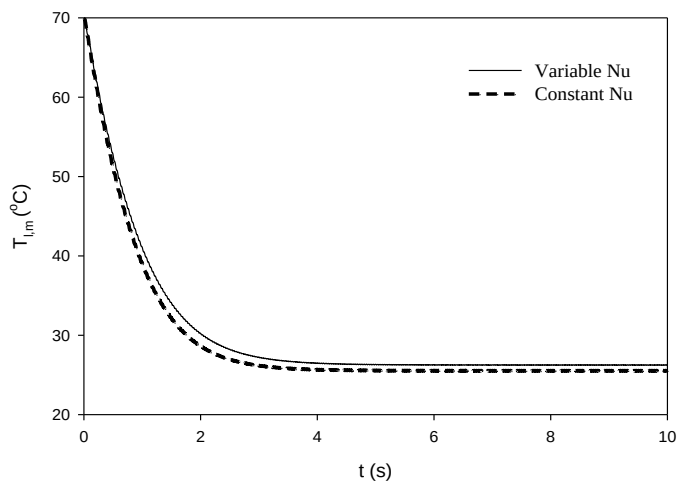

Figure 8 Average mean temperatures of the liquid slug

Figure 9 (a) and (b) show sensible heat transfer into and out from liquid slug for both variable and constant Nu models. After taking the effect of axial variation of surface temperature into account, the sensible heat transferred in and out is almost the same as that of the original model when the flow is turbulent. On the contrary, the sensible heat transfer for the variable Nu model in the laminar region is higher than that for the constant Nu model. The average sensible heat transfer rate is increased from 40.85 for constant Nu model to 42.72W for variable Nu model, which is a 4.5% increase. Thus, the

effect of axial variation of surface temperature for laminar regime on convective heat transfer on the overall heat transfer is important.

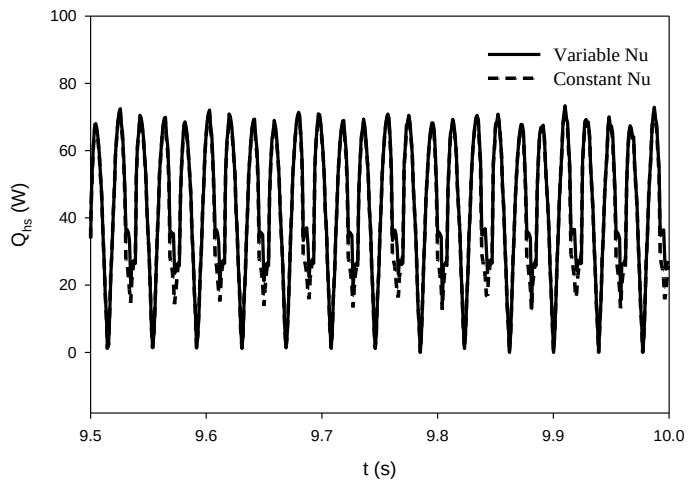

(a) Sensible heat transferred into the liquid slug

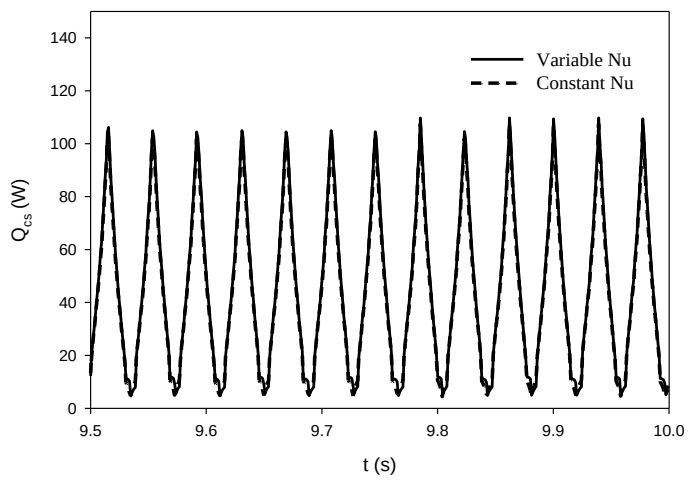

(b) Sensible heat transferred out from the liquid slug

Figure 9 Sensible heat transfer transferred into the liquid slug

2.3.3 The effect of the initial temperatures

The effect of the initial temperatures on the oscillatory flow and heat transfer in the U-shaped minichannel is then studied and the results are shown in Figs. 10 through 15.

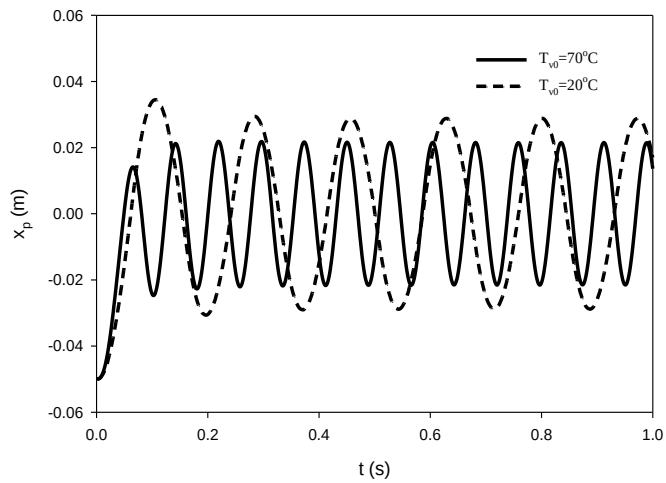

(a) Startup stage

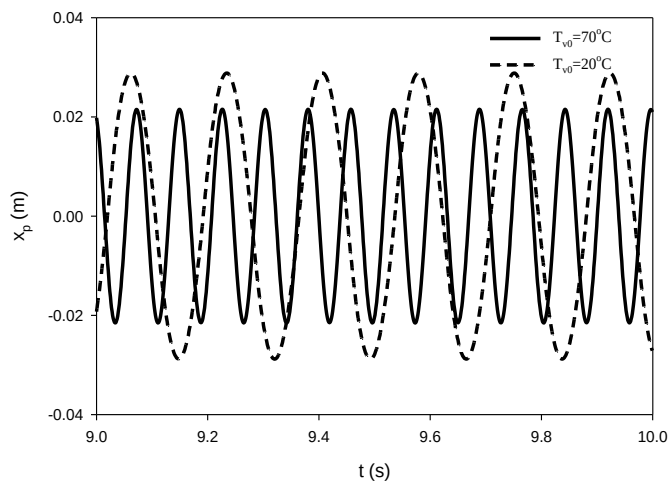

(b) Steady oscillation stage

Figure 10 Displacement of liquid slug for different initial temperature

Figure 10 (a) shows the effect of the initial temperatures of vapor slugs on the displacement of the liquid slugs during the first one second. The decrease of initial temperature has significant effects on the amplitudes and angular frequencies of liquid slug oscillation. The liquid slug exhibited huge fluctuation at the first second and the phase of oscillation also recedes with decreasing temperatures of vapor plugs. Figure 10 (b) shows the effect of the initial temperatures on the displacement of liquid slugs after

steady oscillation is established. The maximum displacement of the liquid slug oscillation with an initial temperature of $20^{\circ}C$ is 0.0288m, which is larger than 0.0214m for the maximum displacement for the initial temperature of 70 °C. The period of liquid slug oscillation is 0.172 second when the initial temperature is 20 °C, which is much longer than the period of 0.077 second when the initial temperature is 70 °C. As a result, the laminar flow plays more important role with lower initial temperature.

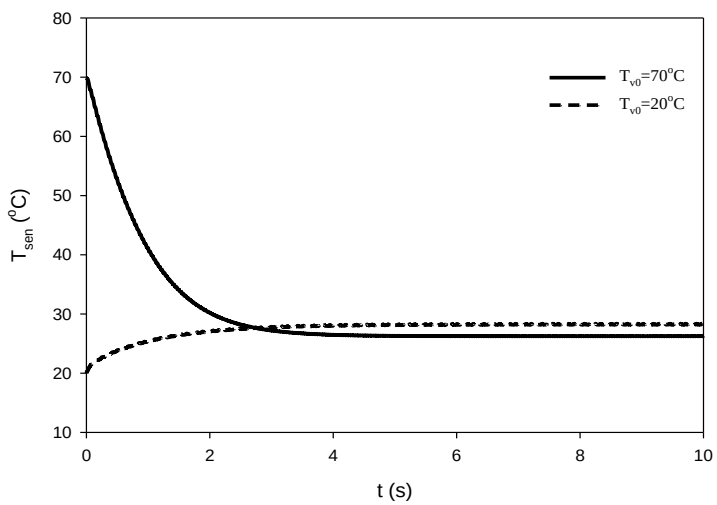

Figure 11 Average mean temperatures of liquid slug for different initial temperature

Figure 11 shows the transient response of average mean temperature of liquid slug to different initial temperature. The steady oscillation was achieved almost at the same time for both cases. However, the liquid temperature for the initial temperature of 20 °C is a little higher than that for the initial temperature of 70 °C.

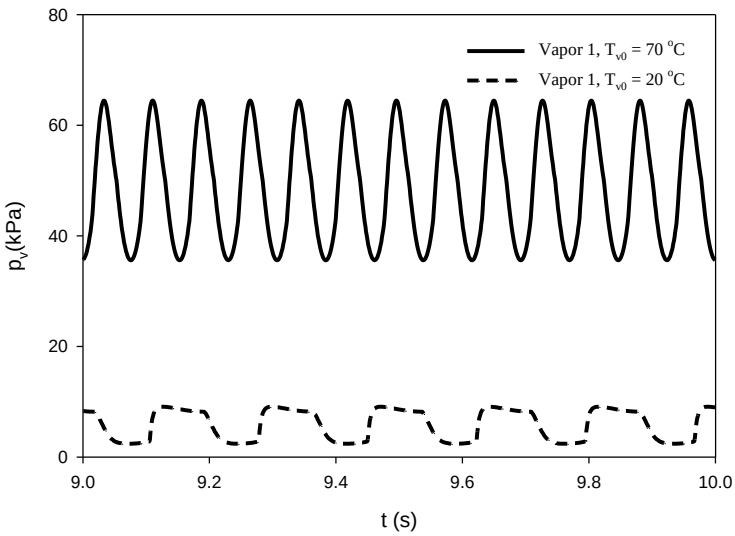

(a) Left vapor plug

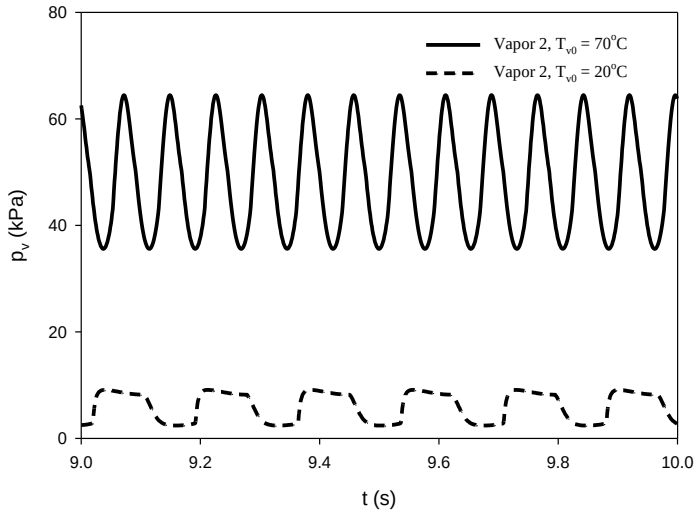

(b) Right vapor plug

Figure 12 Vapor pressures at different initial temperatures

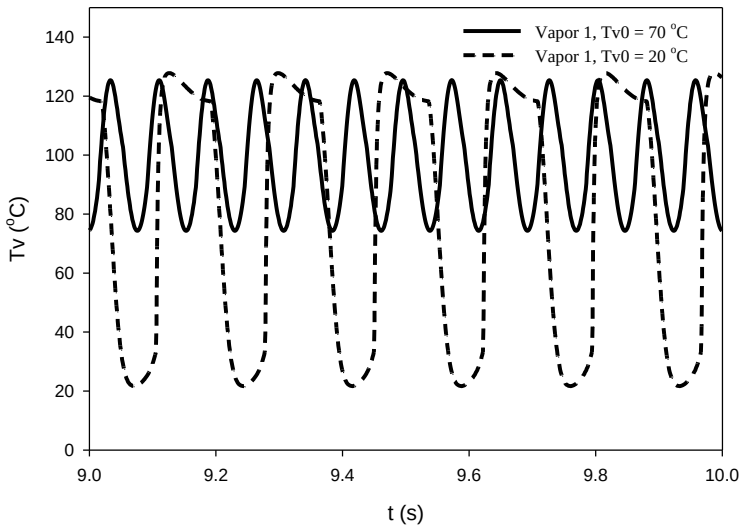

(a) Left vapor plug

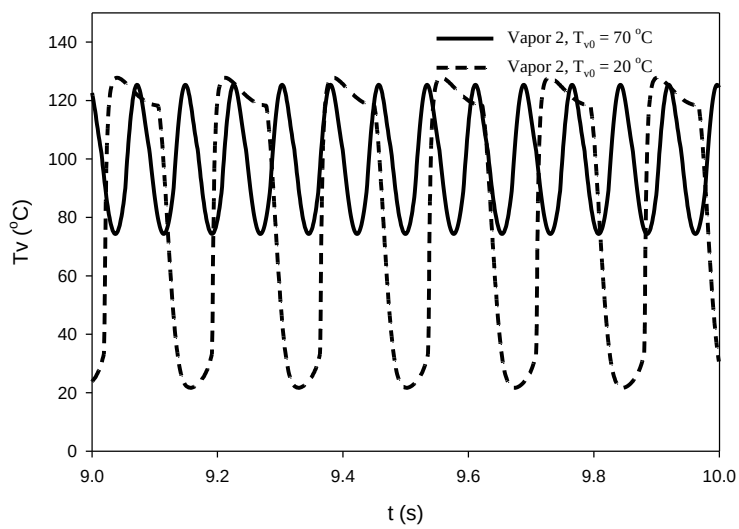

(b) Right vapor plug

Figure 13 Vapor temperatures for different initial temperature

Figure 12 and 13 show the variation of pressures and temperatures for both vapor plugs at different initial temperatures. When the initial temperature is low, the corresponding saturation pressure is low. The saturation pressure corresponding to 20 °C for water is 2336.8 Pa while the saturation pressure for water at 70 °C is 33639Pa. The vapor pressures and temperatures, as shown in Figs. 12 and 13, exhibit similar trends as that of the liquid slug displacement except the oscillating ranges of pressure for different

initial temperatures are different. The amplitude of pressure for initial temperature of 20 °C is much smaller than that for initial temperature of 70 °C. With the same heating and cooling temperatures, the lowest temperatures of the vapor plugs can reach for both different initial temperatures are very different. On the contrary, the highest temperatures of vapor plugs for different initial temperatures are almost the same (see Fig. 8).

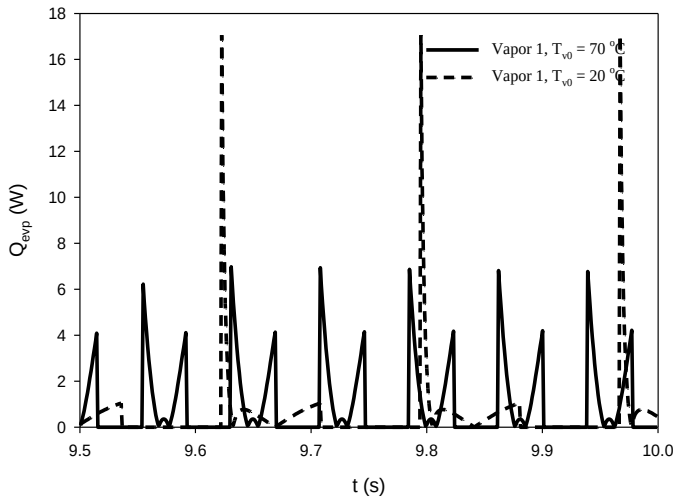

(a) Evaporation

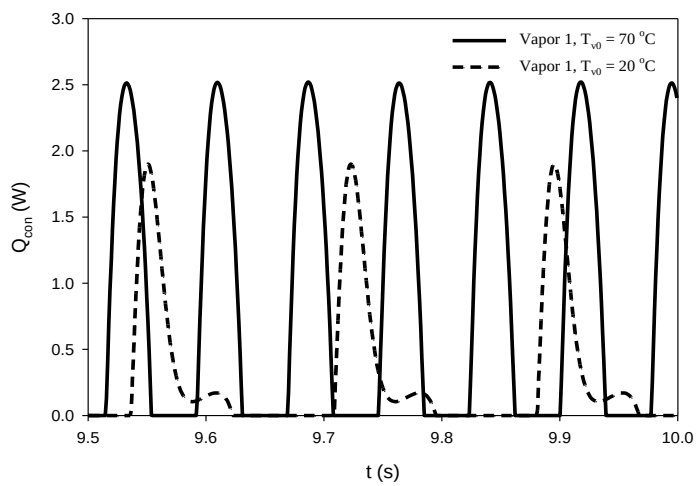

(b) Condensation

Figure 14 Evaporation and condensation of the left vapor plug for different initial temperature

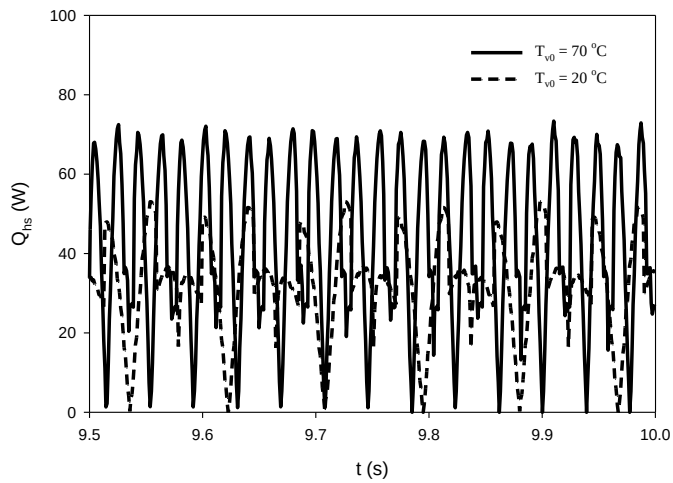

(a) Sensible heat transferred into the liquid slug

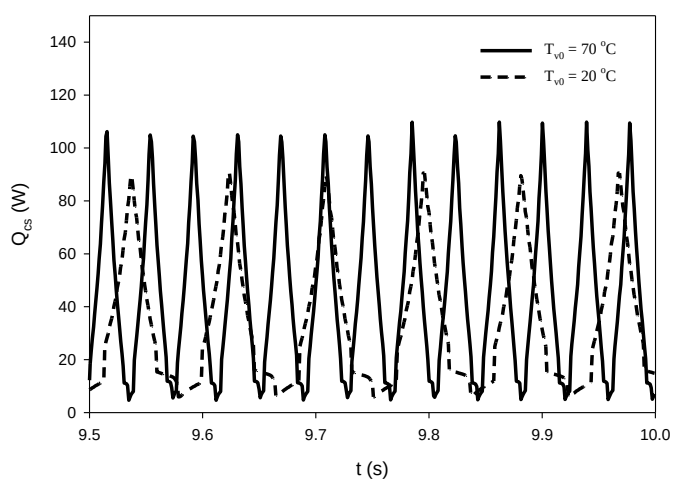

(b) Sensible heat transferred out of the liquid slug

Figure 15 Sensible heat transferred for different initial temperature

Figure 14 shows the effect of the initial temperature on the latent heat transfer. It can be seen from Fig. 14(a) that the latent heat transfer into the vapor experiences a sharp increase in its magnitude is due to large rate of vapor temperature change with time when the liquid moves from left to right. Similarly, the latent heat transferred out of the vapor shown in Fig. 14 (b) experiences a decrease in its magnitude. The sensible heat transferred into and out of the system also exhibits the similar trend as above (see Fig. 15

(a) and (b)), i.e. the sensible heat transfer rate decreases with decreasing initial temperature. The system with initial temperature of 20 °C has lower average heat transfer rate of 32.29 W compared with 42.71 W for the system with an initial temperature of 70°C.

2.4 Conclusions

Heat transfer models in the evaporator and condenser sections of a U-shaped minichannel are developed by analyzing the effects of axial variation of surface temperature, initial temperature of working fluid, and pressure at the bend. The results confirmed that for all cases, heat transfer in an OHP is mainly due to the exchange of sensible heat. The effect of axial variation of surface temperature for laminar regime on the overall heat transfer is important. The effect of initial temperatures of working fluid on the oscillation and heat transfer is very significant. The effect of pressure loss at the bend on the momentum equation of liquid slug is studied and the results show that its effects on the flow motion and heat transfer cannot be neglected. It dampened the oscillating amplitude and slowed down the oscillation.

CHAPTER 3 SURFACE TENSION AND ORIENTATION

3.1 Physical Model

3.1.1 Problem Description

The objective of this chapter is to study the effect of capillary force and orientation on the performance of an oscillating heat pipe. A schematic diagram of the modified physical model is shown in Fig. 16. The geometric parameters and operating conditions remain the same as in Chapter 2, except once the oscillation starts, the contact angles at both ends of the liquid slug will be different, which depend on the direction of liquid slug flow and the inclination angle of the U-shaped tube varies from *0°* to *180°*.

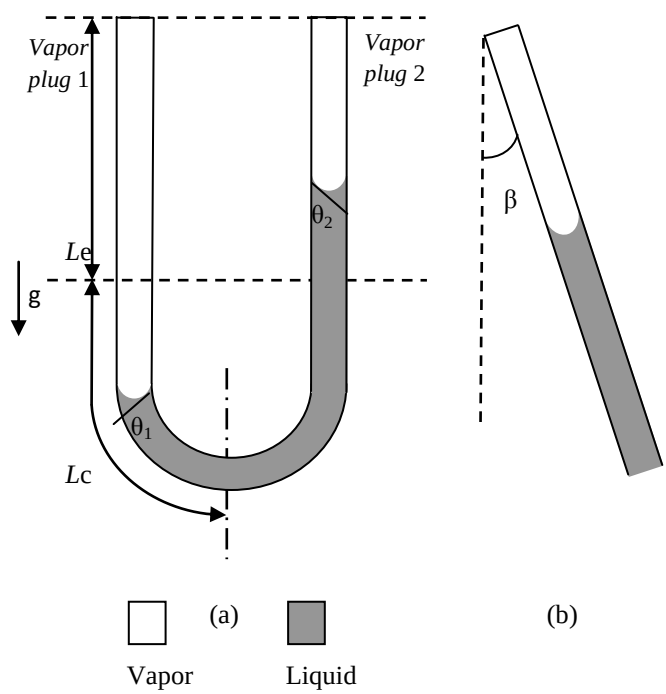

Figure 16 Modified Physical Model

3.1.2 Governing Equations for Oscillatory Flow

The momentum equation for the liquid slug has been changed by adding the effects of capillary force and inclination angle:

$$AL_p\rho_l \frac{d^2x_p}{dt^2} = \left[\left(p_{l1} - p_{l2}\right) - \Delta p_b\right]A - 2\rho_l g\cos\beta A x_p - \pi d L_p \tau_p \tag{47}$$

where the liquid pressures are related to the vapor pressures by Laplace-Young equation:

$$\begin{aligned} p_{v1} - p_{l1} &= \frac{2}{r}\sigma_1\cos\theta_1 \\ p_{v2} - p_{l2} &= \frac{2}{r}\sigma_2\cos\theta_2 \end{aligned} \tag{48}$$

The pressure difference between the two ends of the liquid slug becomes:

$$p_{l1} - p_{l2} = \left(p_{v1} - p_{v2}\right) - \frac{2}{r}\left(\sigma_1\cos\theta_1 - \sigma_2\cos\theta_2\right) \tag{49}$$

where the surface tension is function of temperature. For water, the surface tension can be expressed as:

$$\sigma_i = [75.83 - 0.1477\times(T_{v,i} - 273.15)]\times 10^{-3} N/m \tag{50}$$

The contact angles at two ends depend on the direction of the liquid slug movement. When the liquid slug velocity is positive ($v_p > 0$), the contact angles are $\theta_1 = \theta_{\min}, \theta_2 = \theta_{\max}$ where $\theta_{\min}$ and $\theta_{\max}$ are minimum and maximum contact angle. When the liquid slug velocity is negative ($v_p < 0$), the contact angle becomes $\theta_1 = \theta_{\max}, \theta_2 = \theta_{\min}$.

The rest of governing equations for vapor plugs and heat transfer equations are identical with those in Chapter 2. Hence, the duplicated part of equations is eliminated.

3.2 Results and Discussion

The parameters of the miniature channel are: L_e = 0.1 m, L_c = 0.2 m, L_p = 0.2, d = 0.001m, T_e = 123.4 °C, T_c =20 °C. The initial pressures of the vapor plugs are p_{v0} =31164.64 Pa and the initial temperature of the vapor plug is T_{v0} = 70 °C. The heat transfer coefficient at the heating wall is h_e = 200 W/m^2-K and the heat transfer coefficient at the cooling wall is h_c = 200 W/m^2-K. The two angles $\theta_{\max}$ and $\theta_{\min}$ are respectively set to be equal to be 85° and 33° as the water contacts copper surface. Unless stated otherwise, the above conditions remain the same for each case.

3.2.1 The effect of surface tension

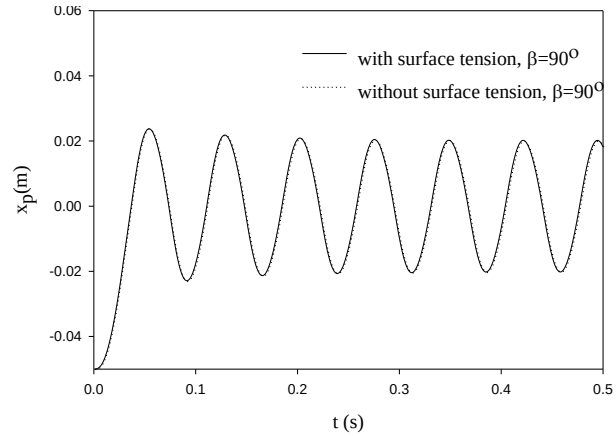

(a) Displacement of liquid slug

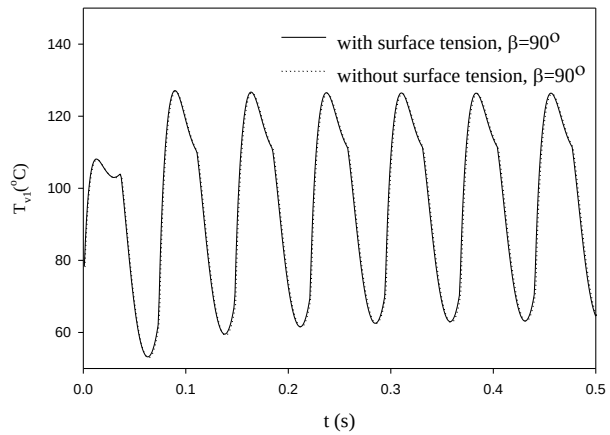

(b) Vapor plug temperatures

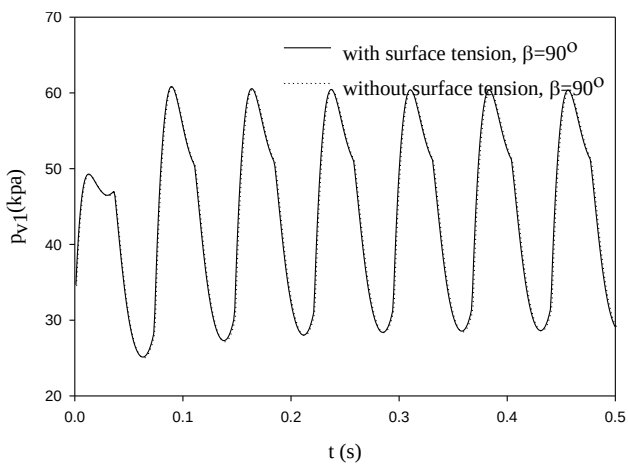

(c) Vapor plug pressure

Figure 17 Comparison of with surface tension and without surface tension at β=90°

Figure 17 (a) shows the comparison of liquid slug displacements for the cases with and without surface tension with β = 90° and d=0.001mm. As can be seen, there is no apparent difference between the displacements for the cases with and without surface tension since the capillary force is relatively small compared with the vapor pressure difference. Figure 17 (b) shows the comparison of left vapor plug temperatures for the cases with and without surface tension. Similar to the trend on liquid slug displacement, there is no effect from surface tension. The comparison of the pressure variations of the left vapor plug for the cases with and without surface tension is shown in Fig. 17 (c). Once again, the vapor plug pressures exhibited the similar trend as the vapor plug temperatures. Therefore, one can conclude that capillary force has little effect on the oscillation flow and heat transfer of an OHP. Although the capillary force is necessary for the formation of the OHP, the performance of the OHP is not affected by the surface tension. The effect of capillary force on the heat transfer was also computed and no noticeable effect was observed.

3.2.2 The effect of orientation

Figure 18 (a) shows the comparison of the displacement of liquid slug for five potential orientations (see Fig. 16 (b)):

(1) $\beta = 0^\circ$ (evaporator above condenser) ,

(2) $\beta = 45^\circ$ (evaporator above condenser) ,

(3) $\beta = 90^\circ$ (horizontally) ,

(4) $\beta = 135^\circ$ (condenser above evaporator) ,

(5) $\beta = 180^{\circ}$ (condenser above evaporator) .

As β increases from 0° to 180°, the gravitational acceleration decreases from +g to –g. As can be seen from this comparison, at other condition being equal, there are an increase of the amplitude and a decrease of the frequency of the oscillation when β increases. The change of amplitude of the liquid slug displacement is so small but the phase is much more delayed as β increases. The frequency of oscillation for the case of β = 180° is decreased compared with that of the case with β = 0°. Figure 18 (b) shows the comparison of left vapor plug temperatures in five different orientations. Similar to the trend on liquid slug displacement, there is a delay in the phase of the vapor temperature with increasing β. The frequency of the temperature oscillation is decreased as β increases. Comparison of the pressure variations of the left vapor plug for five different orientation angles is shown in Fig. 18 (c). It can be seen that the vapor plug pressures in five different orientations exhibited the similar trend as the vapor plug temperatures. Therefore, one can conclude that as β increases, the frequencies of displacement, vapor plug temperature and pressure decrease, while the amplitude slightly increases.

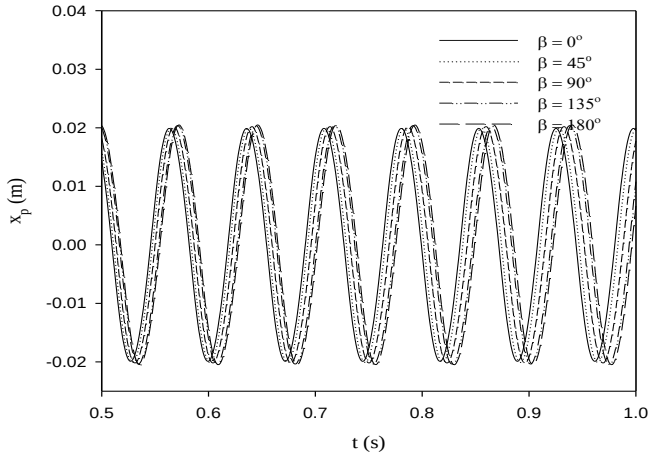

(a) Displacement of liquid slug

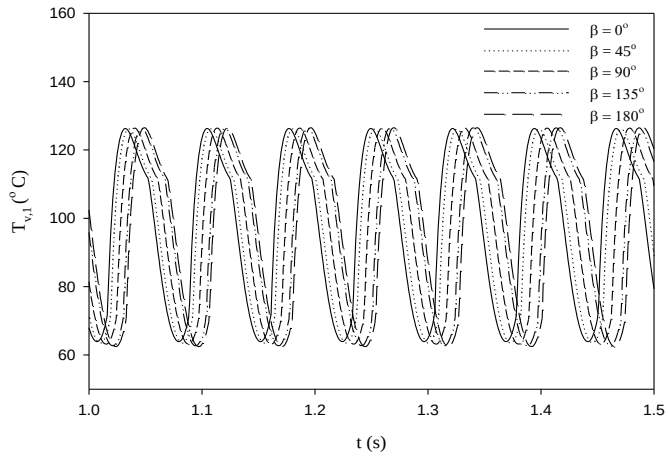

(b) Vapor plug temperatures

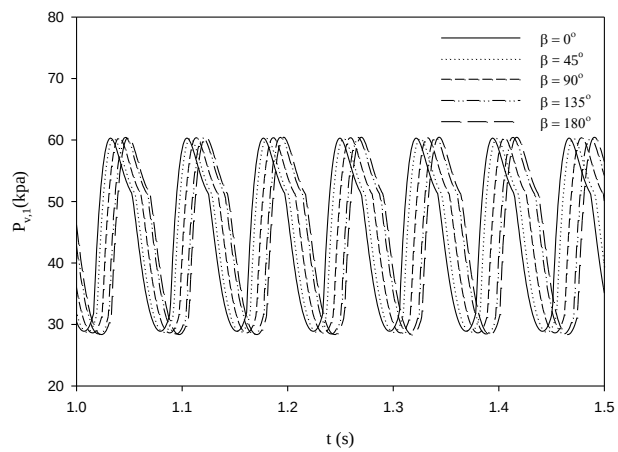

(c) Vapor plug pressure

Figure 18 Comparison of the oscillations of different inclination angles

Figure 19 (a) shows the comparison of sensible heat transfer transferred into the liquid for five orientations. There is a delay of the phase and a slight increase of the of sensible heat transfer in and out of the liquid as β increases. Due to enhanced oscillatory motion of the liquid slug, the average sensible heat transfer rate is increased from 10.95W with β=0° to 11.64W with β=180° – a 6.3% increase. The comparison of latent heat transfer for five different orientations is shown in Fig. 19(b). It is seen that the delay of the phase of the oscillation also results the delay of the phase of evaporation heat transfer but the amplitude of evaporation heat transfer does not increase much. Due to gravity effect, the average evaporation heat transfer increases from 0.49W to 0.50W - a 2% increase. Thus, the effect of gravitational force on the performance of the OHP is very insignificant.

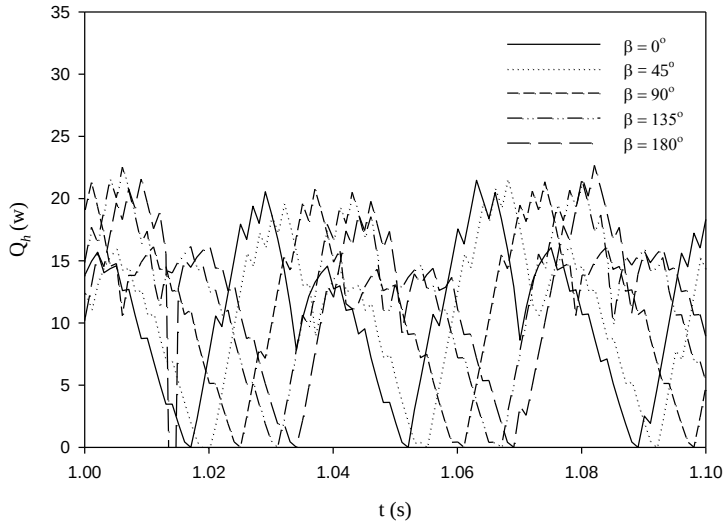

(a) Sensible heat transfer

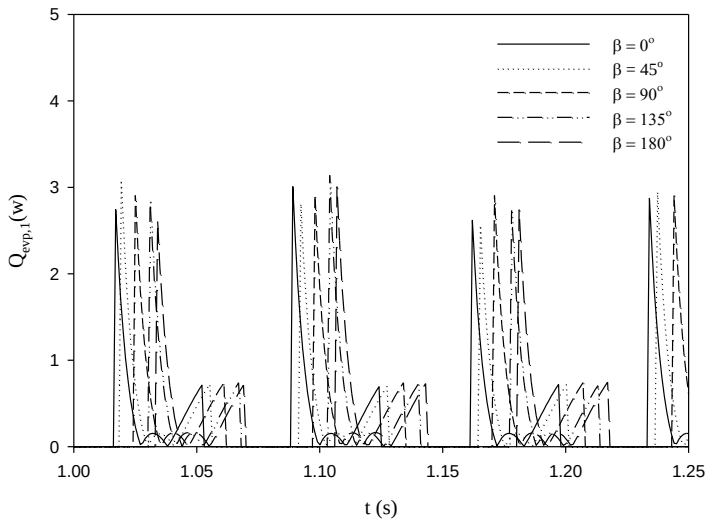

(b) Latent heat transfer

Figure 19 Comparison of heat transfer of different inclination angles

3.2.3 The effect of inner diameter

Figure 20 (a) shows the comparison of the displacement for the cases of five different diameters. As can be seen, at other condition being equal, there are an apparent decrease of the amplitude and an increase of the frequency of the oscillation when the inner diameter decreases together. It can be seen that, the change of amplitude of the liquid

slug displacement is apparent and the phase is much more advanced. The amplitude of oscillation for the cases with d = 0.001 m is decreased compared with that of the case with d = 0.003m. Figure 20 (b) shows the comparison of left vapor plug temperatures for five different diameters. With increasing diameter, the amplitude of temperature oscillation decreases and the phase of oscillation advances. Figure 20(c) shows the comparison of the pressure variations of the left vapor plug in five different diameters. The vapor plug pressures in five different orientations exhibited the similar trend as the vapor plug temperatures.

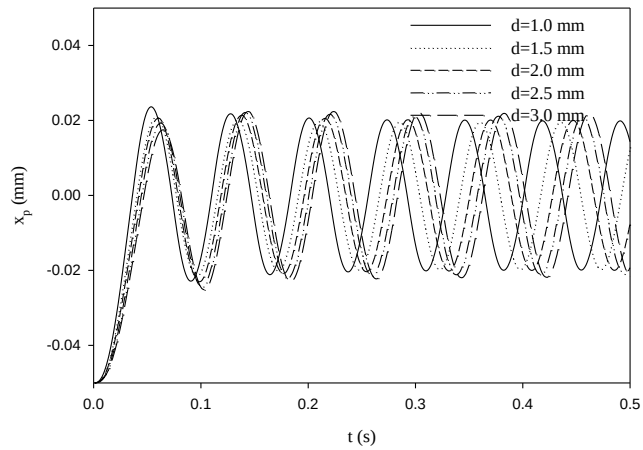

(a) Displacement of liquid slug

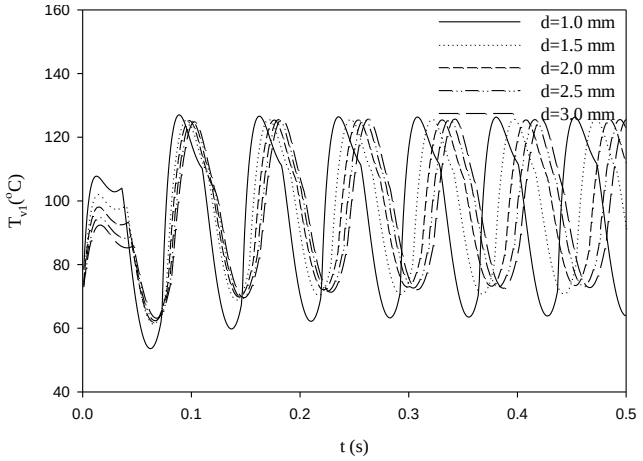

(b) Vapor plug temperatures

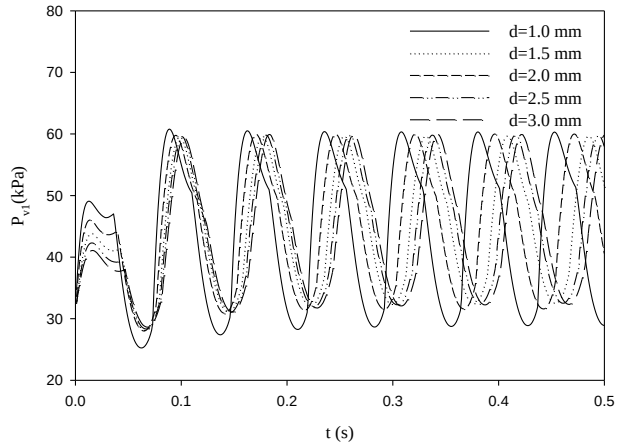

(c) Vapor plug pressure

Figure 20 Comparison of the oscillations for different inner diameters

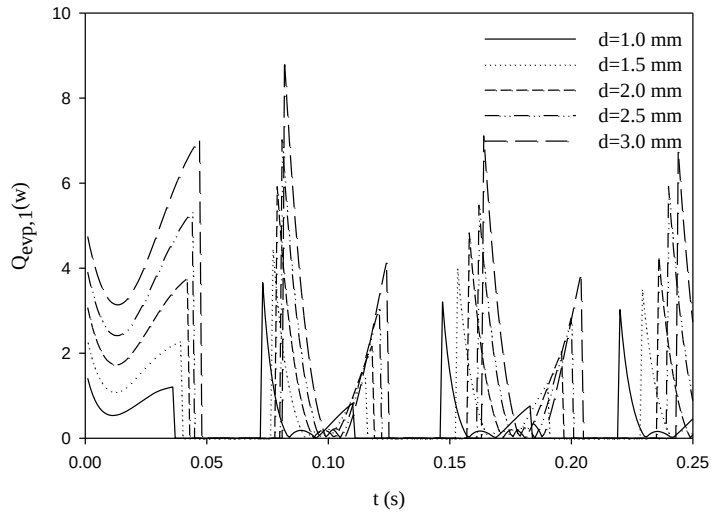

(a) Sensible heat transfer

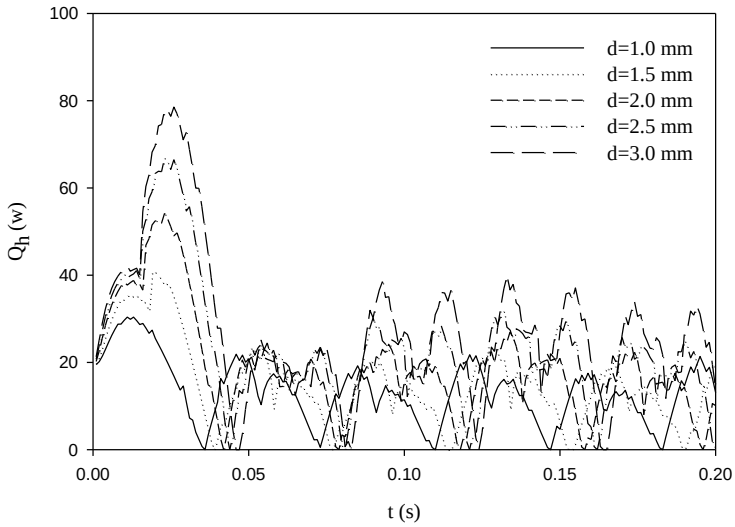

(b) Latent heat transfer

Figure 21 Comparison of heat transfer for different inner diameter

Figure 21(a) shows the comparison of latent heat transfer for different inner diameters. The latent heat transfer increases as the inner diameter increases. Figure 21 (b) shows the comparison of the sensible heat transfer for different inner diameters of OHP. There is an increase of the sensible heat transfer when the inner diameter increases. Although increasing the inner diameter can enhance the heat transfer, the inner diameter must be small enough to ensure formation of liquid slugs in the OHP.

The effect of surface tension on the oscillation can be neglected. The gravitational force has more effect on the frequency of the oscillation than the amplitude. The bottom-heating mode operates most effectively. As the inner diameter of the OHP increases, the heat transfer capability is improved.

3.3 Conclusion

Capillary and gravitational effects on flow and heat transfer of a U-shaped minichannel are fully investigated by comparing displacement of liquid slug, temperature and pressure of vapor plugs latent and sensible heat transfer. The results confirmed that for all cases under the same inner diameter, gravitational force has more effect on the frequency of the oscillation than the amplitude. Besides, the top cooled mode operates most effective. As the inner diameter of the OHP increases, the heat transfer capability is improved. Comparison of the effect with and without surface tension proves that the effect of surface tension on the oscillation can be neglected.

CHAPTER 4 THIN FILM EVAPORATION AND CONDENSATION

4.1 Physical Model

4.1.1 Problem Description

In this chapter, instead of assuming evaporation and condensation heat transfer coefficients, the latent heat transfer due to phase change is calculated by solving the thin film evaporation and condensation. The geometric parameters, operating conditions, governing equations for liquid slug and sensible heat transfer are identical with those in Chapter 2. Therefore, only the derivation of equations for latent heat transfer is presented in detail in this chapter.

4.1.2 Latent Heat Transfer

Figure 22 shows the physical models of film evaporation and condensation heat transfer. With the complication of the two-phase heat transfer in the evaporator and condenser sections, the modeling is divided into two parts: evaporator section and condenser section. In the evaporator section, the liquid film is divided into three regions: nonevaporating region, thin film region and intrinsic meniscus region. In the condenser, the liquid film is divided into two regions: thin film region and intrinsic meniscus region.

In Fig. 22, if the displacement x_p is positive, a relatively flat liquid film is formed the condenser section with an intrinsic meniscus attached and condensation occurs on the flat film and attached meniscus (see Fig. 22 (a)). In the evaporator, when v_p is positive, the liquid slug is moving forward, a thin film is formed and evaporation occurs on the thin

film and meniscus (see Fig. 22 (b)); when v_p is negative, the liquid slug moves backward, a thick film formed and evaporation takes place on the thick film and attached meniscus (see Fig. 22 (c)). The difference between the thick film and the thin film is that the thick film surface is convex [12]. The length of flat thin film in the condenser section, L_1, is calculated from the left end of the condenser to the left end of the liquid the slug accounting for the condensation of the left vapor slug (see Fig.22 (a)); the length of thin film in the evaporator, L_2, is calculated from the transient point to the nonevaporating point (see Fig.22 (b) and (c)). The shape of the meniscus depends on the contact angle which is determined by the direction of the liquid slug movement. Several additional assumptions must be mentioned:

(1) In every time step, liquid and vapor interface is quasi steady state so that equilibrium liquid films can be established.

(2) Heat transport in the microfilm or thick-film is due only to the conduction in the radial direction.

(3) Shear stress at the liquid-vapor interface is negligible.

(4) There are no temperature and pressure gradients in vapor regions.

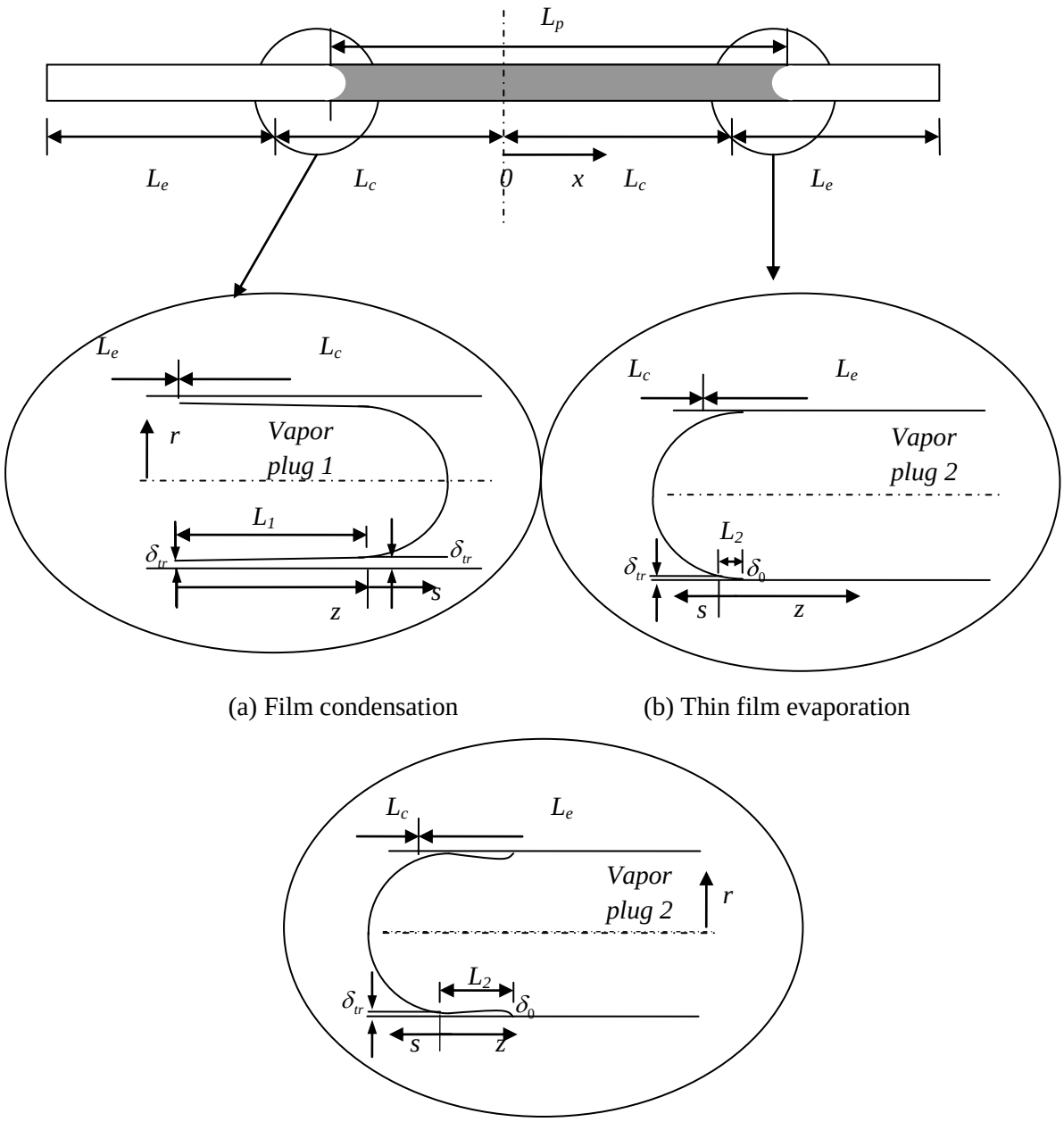

(a) Film condensation (b) Thin film evaporation

(c) Thick film evaporation

Figure 22 Evaporation and condensation models

a. Film Condensation

The physical model of film condensation and the cylindrical coordinate system used in the condenser section are shown in Fig. 22 (a). Both vapor plugs and liquid slug oscillate along the z-coordinate. The mass and energy balances for the liquid film shown in Fig. 22 (a) yield the following:

$$\int_{R-\delta}^{R} r w_l(r) dr = \frac{1}{2\pi\rho_l}\left(\dot{m}_{l,in} - \frac{Q}{h_{lv}}\right) \tag{51}$$

where $\dot{m}_{l,in}$ is the liquid mass flow rate in the inner meniscus region at the transient point, which is supplied by the condensation for $z \geq 0$. $Q(z)$ is the heat flow rate through a given cross section due to condensation from the film for $z \geq 0$ and defined as follows:

$$Q = 2\pi R \int_0^z q_w dz \tag{52}$$

where $q_w(z)$ is the heat flux at the solid-liquid interface due to heat conduction through a cylindrical film with a thickness of δ.

$$q_w = k_l \frac{T_w - T_\delta}{R \ln\left[R/(R-\delta)\right]} \tag{53}$$

where T_δ is the local temperature of the liquid-vapor interface, which differs from the saturated bulk vapor temperature due to the interfacial resistance and effects of curvature and disjoining pressure on saturation pressure over evaporating films. The heat flux across the thin film is defined as [17]:

$$q_\delta = -\left(\frac{2\alpha}{2-\alpha}\right)\frac{h_{lv}}{\sqrt{2\pi R_g}}\left[\frac{p_v}{\sqrt{T_v}} - \frac{\left(p_{sat}\right)_\delta}{\sqrt{T_\delta}}\right] \tag{54}$$

where p_v and $\left(p_{sat}\right)_\delta$ are the saturation pressures corresponding to T_v and at the liquid-vapor interface, respectively. The following two algebraic equations given by the extended Kelvin equation in [17] should be solved to determine T_δ:

$$\left(p_{sat}\right)_\delta = p_{sat}(T_\delta)\exp\left(\frac{\left(p_{sat}\right)_\delta - p_{sat}(T_\delta) + p_d - \sigma K}{\rho_l R_g T_\delta}\right). \tag{55}$$

where K is the local curvature of the liquid-vapor interface. Under steady state conditions, $q_\delta\left(R-\delta\right)/R = q_w$, and it follows from eqs. (53) and (54) that:

$$T_\delta = T_w + \frac{\left(R-\delta\right)}{k_l}\ln\frac{R}{R-\delta}\left(\frac{2\alpha}{2-\alpha}\right)\times\frac{h_{lv}}{\sqrt{2\pi R_g}}\left[\frac{p_v}{\sqrt{T_v}} - \frac{\left(p_{sat}\right)_\delta}{\sqrt{T_\delta}}\right] \tag{56}$$

Equations (55) and (56) determine the interfacial temperature, T_δ, and pressure, $\left(p_{sat}\right)_\delta$, for a given vapor pressure, $p_v = p_{v,sat}\left(T_v\right)$, wall temperature, T_w, and the liquid film thickness, δ. Following Holm and Goplen [18], the disjoining pressure for water can be expressed as

$$p_d = \rho_l R_g T_\delta \ln\left[a\left(\frac{\delta}{3.3}\right)^b\right], \tag{57}$$

where a = 1.5336 and b = 0.0243. Combining eqs.(52) and (53), the following equation is obtained:

$$\frac{dQ}{dz} = 2\pi k_l \frac{T_w - T_\delta}{R \ln\left[R/\left(R-\delta\right)\right]}. \tag{58}$$

The momentum equation for viscous flow in a liquid film is written in the Stokes approximation.

$$\frac{1}{r}\frac{\partial}{\partial r}\left(r\frac{\partial w_l}{\partial r}\right) = \frac{1}{\mu_l}\frac{dp_l}{dz} \tag{59}$$

which is subject to the following boundary conditions:

$$w_l\Big|_{r=R} = 0 \tag{60}$$

$$\frac{\partial w_l}{\partial r}\Bigg|_{(r=R-\delta)} = 0 \tag{61}$$

Solving eq. (59) with boundary conditions specified by eqs. (60) and (61), the velocity profile is obtained as follows:

$$w_l = -\frac{1}{\mu_l}\frac{dp_l}{dz}\left[\frac{1}{4}\left(R^2 - r^2\right) + \frac{\left(R-\delta\right)^2}{2}\ln\frac{r}{R}\right] \tag{62}$$

Substituting eq. (62) into eq.(51), the following equation for the liquid pressure:

$$\frac{dp_l}{dz} = \frac{\mu_l}{2\pi\rho_l F}\left(\frac{Q}{h_{l_v}} - \dot{m}_{l,in}\right) \tag{63}$$

where

$$F=\frac{R^4}{16}+\frac{\left(R-\delta\right)^2}{2}\left[\frac{\left(R-\delta\right)^2}{2}\left(\ln\frac{R}{R-\delta}+\frac{1}{2}\right)-\frac{R^2}{4}+\frac{\left(R-\delta\right)^2}{8}-\frac{R^2}{4}\right] \tag{64}$$

The pressure difference between the vapor and liquid phases is due to capillary and disjoining pressure effects [17]:

$$p_v-p_l=\sigma K-p_d \tag{65}$$

Since the variation of the liquid film thickness in the condenser section is very small, the curvature of the liquid film is expressed as

$$K=\frac{d^2\delta}{dz^2}+\frac{1}{R-\delta} \tag{66}$$

Substituting eqs. (66) and (57) into eq. (65) and differentiating eq. (65) with respect to z, one obtains

$$\frac{d}{dz}\left(p_v-p_l\right)=\frac{d}{dz}\left[\sigma\left(\frac{d^2\delta}{dz^2}+\frac{1}{R-\delta}\right)-\rho_l R_g T_\delta \ln\left[a\left(\frac{\delta}{3.3}\right)^b\right]\right] \tag{67}$$

Since vapor pressure is const in vapor region, the liquid pressure gradient is obtained below:

$$-\frac{dp_l}{dz}=\left[\sigma\left(\frac{d^3\delta}{dz^3}+\frac{1}{\left(R-\delta\right)^2}\frac{d\delta}{dz}\right)-\rho_l R_g T_\delta \frac{b}{\delta}\frac{d\delta}{dz}\right] \tag{68}$$

The third order derivative of film thickness, $\frac{d^3\delta}{dz^3}$, is solved with eqs. (63) and (68), i.e.,

$$\frac{d^3\delta}{dz^3} = \frac{1}{\sigma}\left[\rho_l R_g T_\delta \frac{b}{\delta}\frac{d\delta}{dz} - \frac{\mu_l}{2\pi\rho_l F}\left(\frac{Q}{h_{lv}} - \dot{m}_{l,in}\right)\right] - \frac{1}{\left(R-\delta\right)^2}\frac{d\delta}{dz} \tag{69}$$

In this way, the four first-order ordinary differential equations can be solved using the standard Runge-Kutta procedure, with their respective boundary conditions:

$$\delta' = \frac{d\delta}{dz} \tag{70}$$

$$\delta'' = \frac{d^2\delta}{dz^2} \tag{71}$$

$$\frac{d^3\delta}{dz^3} = \frac{1}{\sigma}\left[\rho_l R_g T_\delta \frac{b}{\delta}\frac{d\delta}{dz} - \frac{\mu_l}{2\pi\rho_l F}\left(\frac{Q}{h_{lv}} - \dot{m}_{l,in}\right)\right] - \frac{1}{\left(R-\delta\right)^2}\frac{d\delta}{dz} \tag{72}$$

$$\frac{dQ}{dz} = 2\pi k_l \frac{T_w - T_\delta}{R\ln\left[R/\left(R-\delta\right)\right]} \tag{73}$$

$$\delta\big|_{z=0} = \delta_{in} \tag{74}$$

$$\left.\frac{d\delta}{dz}\right|_{z=0} = 0 \tag{75}$$

$$\left.\frac{d^2\delta}{dz^2}\right|_{z=0} = 0 \tag{76}$$

$$Q\big|_{z=0} = 0 \tag{77}$$

$$\frac{d\delta}{dz} = 0,\ \frac{d^2\delta}{dz^2} = \frac{1}{R-\delta_{tr}},\ z = L_1 \tag{78}$$

where δ_{in} is unknown and can be determined by solving the above equations iteratively until $\left.\frac{d\delta}{dz}\right|_{z=L_1}=0$ is satisfied. At the same time, the transition film thickness δ_{tr} and the total heat transfer amount for the thin film Q_{c1} are obtained.

Considering the moving contact angle, the thickness beyond the transition point is calculated by

$$R' = \left(R - \delta_{tr}\right) / \cos\theta \tag{79}$$

$$\delta_{me} = R - \sqrt{R'^2 - \left(\left(R - \delta_{tr}\right)\tan\theta + s\right)^2} \ . \tag{80}$$

The heat transfer in the meniscus region is then

$$Q_{c2} = 2\pi R k_l (T_{v,i} - T_c) \int_0^{R_L} \frac{1}{\delta_{me}} ds \tag{81}$$

The total condensation heat transfer amount for the condenser is

$$Q_{cond} = Q_{c1} + Q_{c2} \tag{82}$$

b. Thin Film Evaporation

Modeling of the thin film evaporation is similar to the thin film condensation, but the thin film is thinner and therefore the Cartesian coordinate system is used to simplify the model. The simplified physical model of thin film evaporation in the evaporator section is shown in Fig. 22 (b). The liquid film thickness in the evaporator section satisfies [6]:

$$\frac{d}{dz}\left(\sigma K - p_d\right) = \frac{3\mu_l}{2\pi R \rho_l \delta^3}\left(\dot{m}_{l,in} - \frac{Q}{h_{lv}}\right) \tag{83}$$

where the curvature of the liquid film, K, is calculated by

$$K = \frac{d^2\delta}{dz^2}\left[1 + \left(\frac{d\delta}{dz}\right)^2\right]^{-3/2} \tag{84}$$

and the disjoining pressure, p_d, is the same as in condensation model. Q in eq. (83) is the heat flow rate through a given cross section due to evaporation from the film for $z \geq 0$ and defined as follows:

$$Q = 2\pi R \int_0^z \frac{k_l (T_e - T_\delta)}{\delta} ds \tag{85}$$

Instead of considering the third-order ordinary differential equation (83), the following four first-order equations including four unknown variables: δ, Δ, p_{cap} and Q should be considered using the standard Runge-Kutta procedure with their respective boundary conditions:

$$\frac{d\delta}{dz} = \Delta \tag{86}$$

$$\frac{d\Delta}{dz} = \left[1 + \left(\Delta\right)^2\right]^{3/2}\left(\frac{p_{cap} + p_d}{\sigma}\right) \tag{87}$$

$$\frac{dp_{cap}}{dz} = -\frac{3\mu}{\rho_l h_{lv} \delta^3} Q\left(z\right) \tag{88}$$

$$\frac{dQ}{dz} = \frac{k_l (T_e - T_\delta)}{\delta} \tag{89}$$

$$\delta\big|_{z=0} = \delta_0, \tag{90}$$

$$\Delta\big|_{z=0} = 0, \tag{91}$$

$$p_{cap}\big|_{z=0} = -\frac{\sigma}{R-\delta_0} - p_d, \tag{92}$$

$$Q\big|_{z=0} = 0, \tag{93}$$

where δ_0 is the nonevaporating film thickness calculated by the following equation

$$\delta_0 = 3.3\left\{\frac{1}{a}\exp\left[\frac{p_{sat}(T_w) - p_v\sqrt{T_w / T_v} + \sigma K}{\rho_l R_g T_w} + \ln\left(\frac{p_v}{p_{sat}(T_w)}\sqrt{\frac{T_w}{T_v}}\right)\right]\right\}^{1/b} \tag{94}$$

Following the approach by Khrustalev and Faghri [19] for prediction of evaporation from a hemispherical liquid-vapor meniscus with a radius of $R - \delta_{tr}$ and considering effect of the moving contact angle, the vapor velocity at $z = 0$, $\bar{w}_{v,in}$ can be defined as

$$\bar{w}_{v,in} = \frac{2}{h_{lv}\rho_v\left(R-\delta_{tr}\right)}\int_0^{R_L}\frac{T_w - T_\delta}{\delta / k_l}\times\sin\left[\arccos\frac{s}{R-\delta_{tr}}\right]ds \tag{95}$$

where $R_L = R' - \left(R - \delta_{tr}\right)\tan\theta$.

Therefore, the total amount of heat transfer through meniscus can be obtained using,

$$Q_{e2} = \rho_v A \bar{w}_{v,in} h_{lv} \tag{96}$$

where s is the coordinate along the solid-liquid interface, shown in Fig. 22 (b), and the liquid film thickness, δ, for $s \geq 0$ is calculated by eqs. (79) and (80).

As the thin film thickness increases, the thin film is considered to transform into meniscus when the disjoining pressure drops to its 1/1000 of its value at non-evaporating film. Meanwhile, with the transient film thickness the total evaporative heat transfer amount for the entire thin film Q_{e1} is obtained and Q_{e2} is solved by eq. (96). The total evaporative heat transfer for the evaporator section is

$$Q_{evp,i} = Q_{e1} + Q_{e2} \tag{97}$$

c. Thick film evaporation

The physical model of thick film evaporation and the cylindrical coordinate system used in the evaporator section are shown in Fig. 22 (c). The modeling of the thick film evaporation is similar to the thin film condensation so that the general equations can be used to describe evaporation.

The mass and energy balances for the liquid film shown in Fig. 22 (c) can be calculated by eq. (51). Here, $\dot{m}_{l,in}$ is the liquid mass flow rate in the inner meniscus region at $z = 0$, which supplies the evaporating film with liquid for $z \geq 0$. $Q(z)$ is the heat flow rate through a given cross section due to evaporation from the film for $z \geq 0$ and defined as in Eq. (52) and (53). Following the same procedure as in condenser section we obtain the following equation:

$$\frac{dp_l}{dz} = \frac{\mu_l}{2\pi\rho_l}\left(\frac{Q}{h_{lv}} - \dot{m}_{l,in}\right) \times \left[\frac{R^4}{16} + \frac{(R-\delta)^2}{2}\left(F + \frac{(R-\delta)^2}{8} - \frac{R^2}{4}\right)\right]^{-1} \tag{98}$$

where

$$F = \frac{(R-\delta)^2}{2}\left(\ln\frac{R}{R-\delta} + \frac{1}{2}\right) - \frac{R^2}{4} \tag{99}$$

Introducing the slope of thick film

$$d\delta / dz = \Delta \tag{100}$$

one can obtain

$$\frac{d\Delta}{dz} = \left[1 + (\Delta)^2\right]^{3/2}\left(\frac{p_v - p_l + p_d}{\sigma} - \frac{\cos(\arctan\Delta)}{R-\delta}\right). \tag{101}$$

The four first order differential equations, eqs. (73), (98) , (100) and (101) include four unknown variables: δ , Δ , p_l and Q . Therefore, four boundary conditions are set forth at $z = 0$:

$$\delta = \delta_{tr} \tag{102}$$

$$\Delta = 0 \tag{103}$$

$$p_l = p_{v,i} - \frac{\sigma}{R - \delta_{tr}} + p_d \tag{104}$$

$$Q = 0 \tag{105}$$

The boundary conditions specified in eqs. (103) and (104) were obtained from the assumptions that the pressure variation in the meniscus liquid is negligible compared to the capillary pressure and that the meniscus smoothly transforms into a liquid film. The boundary condition (105) directly follows from eq. (52). There are also three parameters, δ_{tr} , $\dot{m}_{l,in}$ and $\bar{w}_{v,in}$ and an additional variable T_δ involved in this problem. They will be considered using additional algebraic equations and some constitutive boundary conditions including those at the end of the liquid film ($z = L_2$).

The liquid film inevitably ends with a microfilm (Fig.22 (c)) so that its thickness at $z = L_2$ is very small so that the disjoining pressure is very important in the microfilm region allowing the local interface temperature, T_δ to approach T_w , suppressing evaporation. On the contrary, δ_{tr} is expected to be thick enough for the disjoining pressure to be zero. At the end of the microfilm ($z = L_2$) the liquid film is nonevaporating ($T_\delta = T_w$) with the length of δ_0 .

The parameter $\dot{m}_{l,in}$ should be found using a constitutive boundary condition at the end of the microfilm.

$$\dot{m}_{l,in} = \left. \frac{Q}{h_{lv}} \right|_{z=L_2} \tag{106}$$

which states that the liquid mass flow rate $z = L_2$ is zero and is consistent with Eq. (51).

The above equations and with the boundary conditions have been solved using the standard Runge-Kutta procedure and the shooting method on parameter $\dot{m}_{l,in}$ to satisfy Eq.

(106). Algebraic equations (55) and (56) with two unknowns, $(p_{sat})_\delta$ and T_δ, have been solved numerically for every point on z using a Wegstein's iteration method [20]. All the unknown variables were found with the accuracy of 0.0005 percent. During the numerical procedure, the step size of *dz* was 10^{-7} m, and the thermophysical properties of the saturated vapor and liquid were recalculated for each of the points at the corresponding vapor temperature T_v. L_2 was determined by checking if δ was approaching δ_0 at the end of the thick film and the total evaporative heat transfer amount for the entire thick film Q_{e1} is obtained. With the heat transfer through the meniscus region, the total evaporative heat transfer for the evaporator section is obtained.

4.2 Numerical Procedure

The governing equations in the above physical model can be solved numerically. An explicit finite difference scheme is employed to solve the governing equations of the vapor plugs and the liquid slug. An implicit scheme with uniform grid [16] is employed to solve transient heat transfer in the liquid slug. The results of each time-step can be obtained by the numerical procedure outlined below:

1) Assume the temperatures of the two vapor plugs T_{v1} and T_{v2}, and calculate thermal and physical properties of liquid according to T_l

2) Check the moving direction of the liquid slug. If the liquid slug is moving forward, solve for Q_{evp} and $Q_{cond,}$ from thin film evaporation and condensation models with meniscus; if the liquid slug is moving backward, solve Q_{evp} and $Q_{cond,}$ from thick film evaporation and thin film condensation models with meniscus.

3) Obtain the new masses of the two vapor plugs m_{v1} and m_{v2}, by accounting for the change of vapor masses from eqs. (25) and (26).

4) Calculate the pressure of the two vapor plugs, p_{v1} and p_{v2}, from eqs. (21) and (22).

5) Solve for T_{v1} and T_{v2} from eqs. (23) and (24).

6) Solve for x_p from eq. (1).

7) Compare T_{v1} and T_{v2} obtained in Step 6 with assumed values in step 1. If the differences meet the small tolerance, then go to the step 8; otherwise, the above procedure is repeated until a converged solution is obtained.

8) Solve for liquid temperature distribution from eq. (36) and calculate Q_h and Q_c with eqs. (45) and (46).

After the time-step independent test, it was found that the time-step independent solution of the problem can be obtained when time-step is $\Delta t = 1\times10^{-3}$ s, which is used in all numerical simulations.

4.3 Results and Discussion

The following parameters is used in this chapter to simulate the vertically U-shaped minichannel with: $L_e = 0.1m$, $L_c = 0.1m$, $L_p = 0.2m$, $d = 3.34mm$, $T_e = 100^\circ C$, $T_c = 60^\circ C$, $p_0 = 47359$Pa, $T_0 = 80^\circ C$, $\theta_{\min} = 33^\circ$ and $\theta_{\max} = 85^\circ$. Unless stated otherwise, the above conditions remain the same for each case.

Figure 23 shows the variation of liquid slug displacement, x_p, vapor pressure, p_v, and the vapor temperature, T_v, with time when $T_e = 90^\circ C$ and $T_c = 70^\circ C$. The period of the oscillation of the liquid slug is 0.081 s and amplitude of the displacement of the liquid slug is 0.009 m. The highest and lowest temperatures of vapor plugs are 89.99 °C and 73.08 °C, respectively; the largest temperature drop between wall and vapor is only 17 °C. The corresponding highest and lowest saturated vapor pressures are 53,550 Pa and 43,552 Pa.

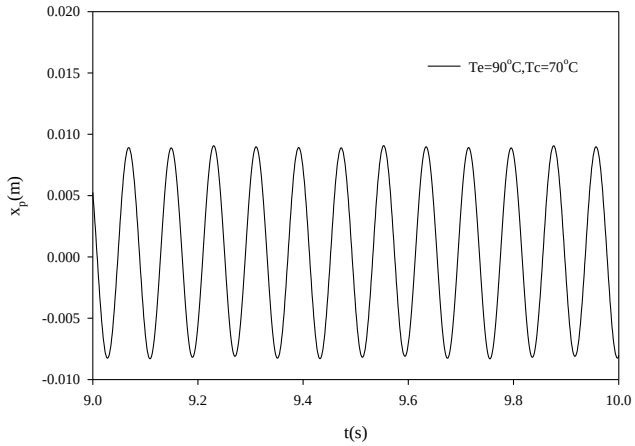

(a) liquid slug displacement

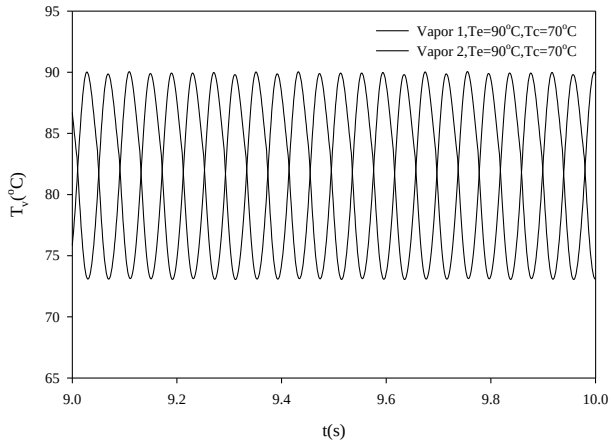

(b) vapor temperature

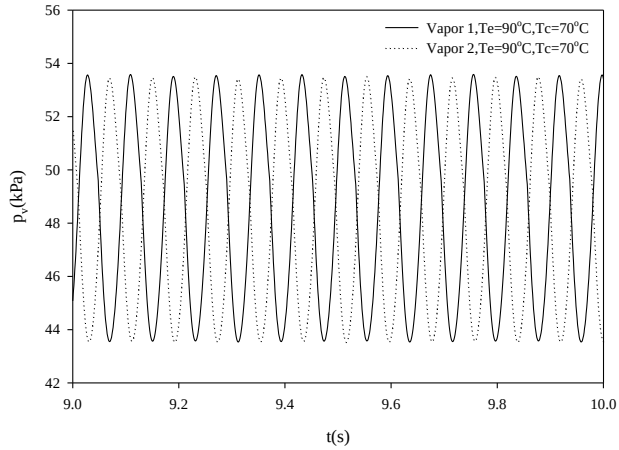

(c) vapor pressure

Figure 23 Variation of liquid slug displacement, vapor pressure and temperature

Figure 24 (a) shows latent heat transfer into and out from the left vapor plug. It can be seen that when the left end of the liquid slug moves into the evaporator section, the evaporative heat transfer of vapor 1 starts at a small rate which is due to thin film and meniscus heat transfer mode. When the liquid slug reaches the leftmost point and then moves backward, the rate of evaporation increases sharply due to the thick film heat transfer mode as the liquid slug moves back and vapor temperature drops. As the vapor 1 expands, its temperature drops and the rate of evaporation increases until the left end of the liquid slug moves into the condenser section where condensation occurs. The thin film condensation of vapor 1 starts and the condensation rate gradually increases since the length of condensation film increases when the liquid slug moves to the right. Meanwhile, due to condensation and expansion, the vapor temperature decreases incessantly and hinders condensation. Therefore, the rate of condensation first reaches its maximum value and then decreases to its minimum value after liquid slug approaches the rightmost point. When the liquid slug moves back, the temperature of vapor 1 decreases slightly and again raises due to compression, as a result, the condensation rate increases again. However, as the liquid slug returns to the evaporator section, the length of the condensation film decreases to zero, condensation stops and evaporation starts again. As can be seen, the length of the condensation film and temperature difference determine the condensation rate; the temperature difference and the film thickness determine the evaporation rate because the thickness of evaporation film is small compared with that of thin film condensation.

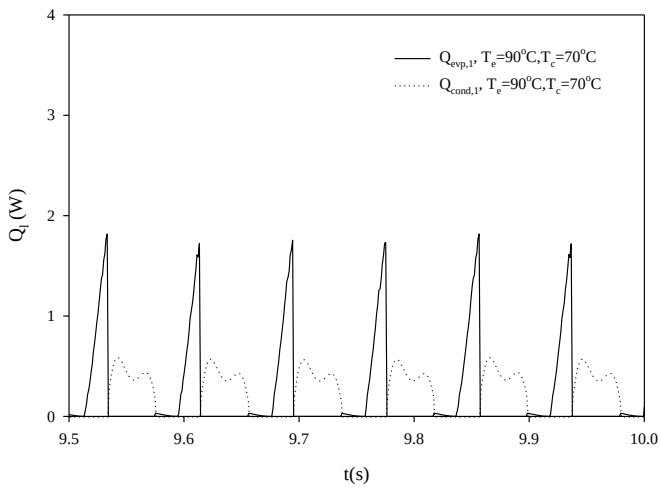

(a) Latent heat transfer of Vapor 1

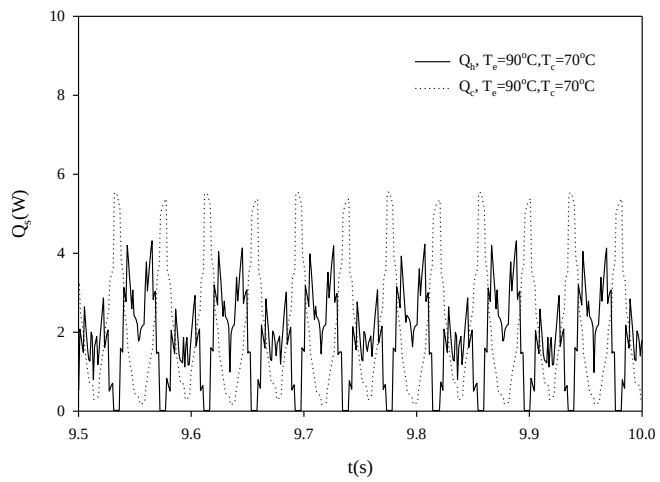

(b) Sensible heat transfer of liquid slug

Figure 24 Latent heat transfer of Vapor plug 1 and sensible heat transfer of liquid slug

Figure 24 (b) shows sensible heat transfer into and out from the liquid slug. It can be seen that the contribution of sensible heat on the total heat transfer amount is larger than that of latent heat. The average heat transferred due to evaporation and condensation for one period of the heat pipe operation is 0.46W. The average sensible heat transfer for the same time period is 2.01 W, which represents an overall contribution of 81.8 %. It can be concluded that heat transfer in an OHP is mainly due to the exchange of sensible heat. The role of thin film evaporation and condensation on the operation of OHPs is mainly

on sustaining the oscillation of liquid slug so that heat transfer is highly enhanced although the contribution of latent heat on the overall heat transfer is not significant.

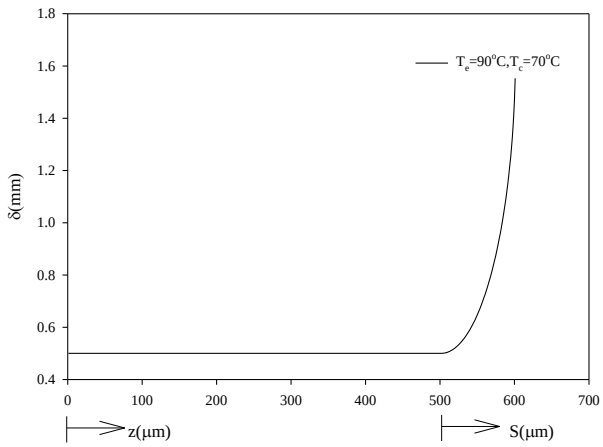

(a) Condensation film thickness

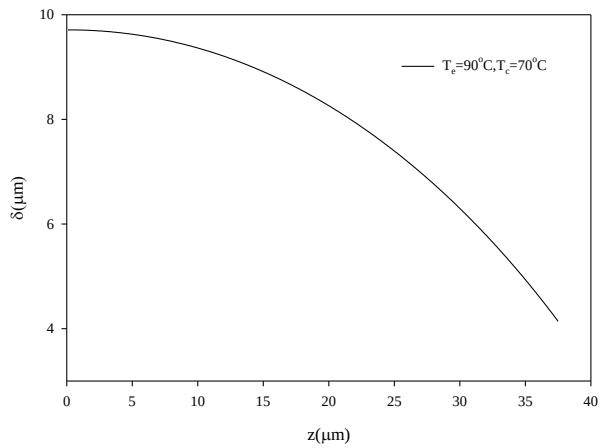

(b) Thin evaporating film

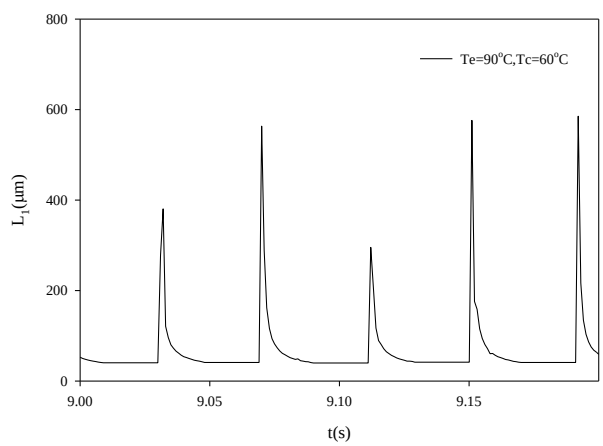

(c) Variation of the length of thick evaporating film

Figure 25 Condensation and evaporation film thickness profiles versus z coordinates and the length variation with time of the thick film

Figure 25 shows the length of condensation and evaporation film thickness profiles versus z coordinates and the length variation of the thick film with time. In Fig. 25 (a), a flat thin condensation film is formed before the meniscus and the film starts with a thickness that satisfies the length of the liquid film as well as the energy and mass balances. The averaged thickness of the flat thin film is around $100\mu m$ through which heat flux is 1000W/m^2 and accumulative condensation rate is 0.46W. In Fig. 25 (b) the thin film region of the liquid film is clearly demonstrated but the thickness of the thin film is very small ($\sim 1\mu m$) and short ($\sim 36\mu m$) comparing with the condensing film. It is this short and thin film transfers 0.46 W while the long and thick condensing film transfers the same amount of heat. It can be seen in Fig. 25 (c) that the length of thick film is longer with smaller temperature difference between vapor plug and evaporator and shorter with larger temperature difference. Because when the temperature difference is high, the heat flux through the thick film is so high that most of the liquid supplied evaporates and cannot maintain the same length of the thick film. On the contrary, with small temperature difference the heat flux through the thick film is low so that sufficient liquid flows into the thick film and maintains a longer thick film. Although the length of the thick film with lower temperature difference is longer, the actual cumulative evaporation rate is small compared with that with shorter thick film length and larger temperature difference. Since the thickness of the thick film varies around 1 micron, high temperature difference results in extremely high heat flux which is about 10^5 W/m^2. Temperature difference is necessary for the high heat transfer through such a thick-film but too large temperature difference restrains the formation of the thick film as it dries out the liquid film.

The influences of the evaporator temperature and the inner diameter on the oscillatory flow and heat transfer are then studied and the results are shown in Figs. 26 and 27. Figure 26(a) shows the effect of the evaporator temperature on the displacement of the liquid slugs. The increase of evaporator temperature has significant effects on the amplitudes and frequencies of liquid slug oscillation. When the temperature difference between evaporator and condenser is high, the vapor pressure varies in a larger range according to the temperature range so that larger pressure difference can be provided. As a result, the amplitude of oscillation is larger when evaporator temperature is higher. The maximum displacement of the liquid slug oscillation with evaporator temperature of 120 °C is 0.0217m, which is larger than 0.0163 m and 0.0194 m – the maximum displacements when the evaporator temperatures are 100°C and 110°C, respectively. The period of liquid slug oscillation is 0.080 second when the evaporator temperature is 100 °C, which is longer than the periods of 0.077 second and 0.079 second when the initial temperatures are 120°C and 110°C, respectively. Based on the period and amplitude of the liquid slug, it can be calculated that the average liquid slug velocities are 0. 804 m/s, 0.982 m/s and 1.127 m/s for 100 °C, 110°C and 120°C, respectively. The increase of the evaporator temperature accelerated the oscillation and enhanced forced convection heat transfer.

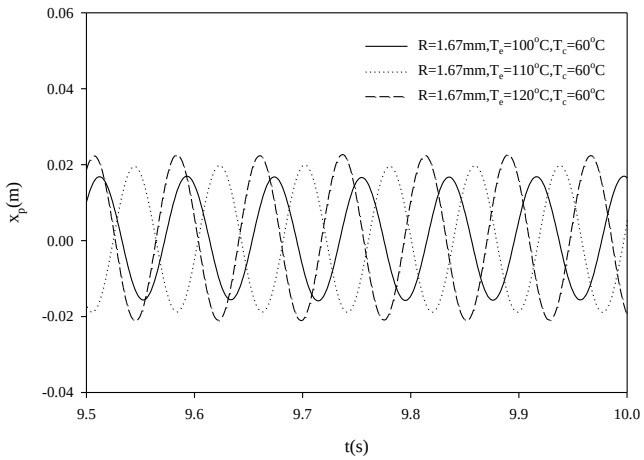

(a) Liquid slug displacement

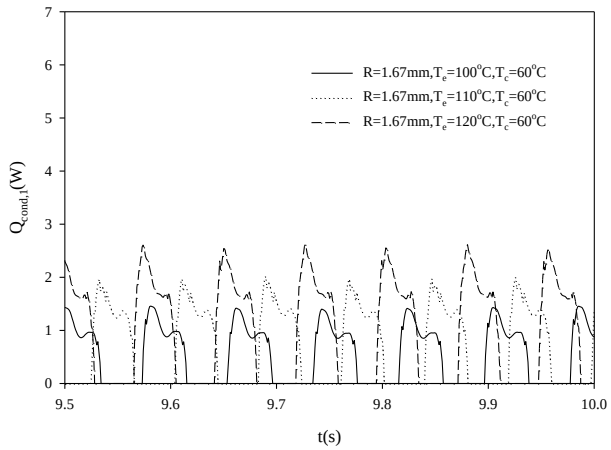

(b) Condensation heat transfer

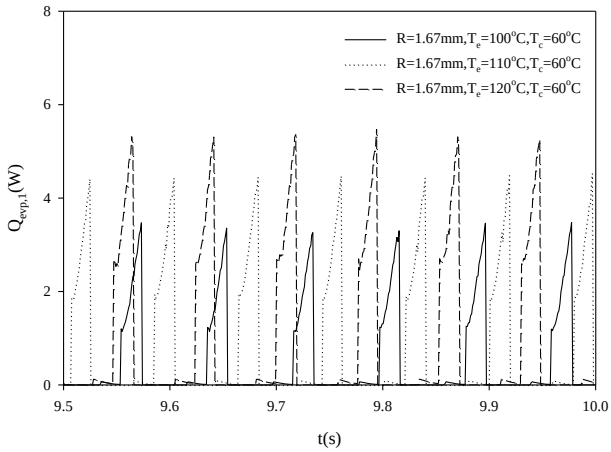

(c) Evaporation heat transfer

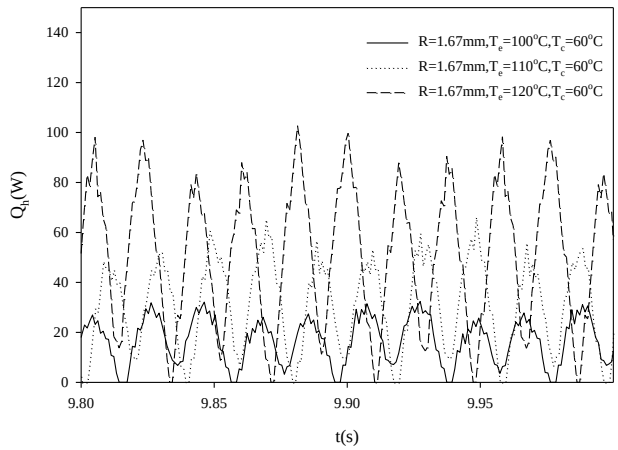

(d) Sensible heat transfer in

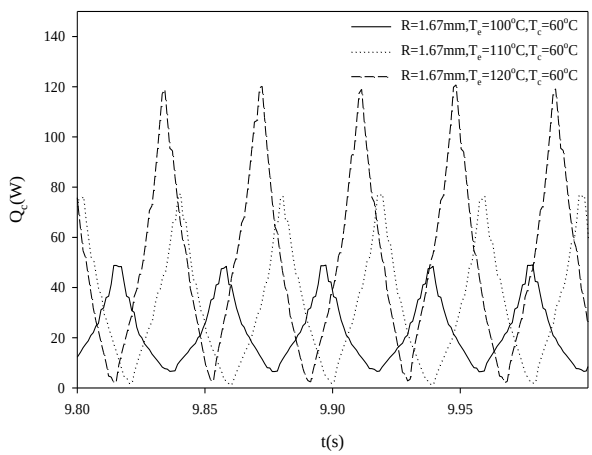

(e) Sensible hear transfer out

Figure 26 Influence of the evaporation temperature on the performance of the OHP

Figure 26 (b), (c), (d) and (e) shows the influence of the evaporator temperature on the latent heat transfer of vapor 1 and the sensible heat transfer of the liquid slug. It can be seen from Figure 26 (b) that the latent heat transfer out of the vapor experiences a sharp increase in its magnitude with the increase of the evaporator temperature. Similarly, the latent heat transferred into the vapor shown in Fig. 26 (c) experiences an increase in its magnitude. The sensible heat transferred into and out of the system also exhibits the similar trend as above (see Fig. 26 (d) and (e)), i.e. the sensible heat transfer rate increases with increasing evaporator temperature. The system with evaporator

temperature of 120 °C has higher average heat transfer rate of 52.59W compared with 20.95 W and 33.54 W for the system with evaporator temperatures of 100°C and 110°C, respectively.

Figure 27 (a) shows the influence of the inner diameter on liquid slug displacement. To study the effect of diameter on OHP performance, three different inner diameters of the tube are investigated: 2 mm, 3.34 mm and 4 mm. Figure 27 (a) shows the amplitude of oscillation of the liquid slug decreases and the frequency of the oscillation of the liquid slug increases when the diameter of the tube decreases. The amplitude of liquid oscillation decreases with increasing diameter: for the three diameters studied, the amplitudes are 0.0171m, 0.0163 m and 0.0158 m, respectively. The periods of the oscillation for the three diameters are 0.082 s, 0.081 s, and 0.080 s, respectively, i.e., the difference between these three cases is not significant. The decrease of diameter has lesser effect on the frequency than on the amplitude of liquid slug displacement. The variation of the diameter of the minichannel has great effects on both latent and sensible heat transfer. Fig. 27 (b) and (c) show the average latent heat transfer rate for the diameter of 2 mm is 0.586 W which is a 55.3 % decrease from 1.31W for the diameter of 4 mm and a 50.7 % decrease from 1.06W for the diameter of 3.34 mm. Figure 27 (d) and (e) shows the effect of the diameter of the minichannel on the sensible heat transferred into and out of the liquid slug. The average sensible heat transfer rate for the diameter of 2 mm is 11.6W which is a 48.1% decrease from 22.35 W for the diameter of 4 mm and a 41.4 % decrease from 19.8 W for the diameter of 3.34 mm. The decrease of total heat transfer rate is mainly due to the decrease of heat transfer area of the miniature tube.

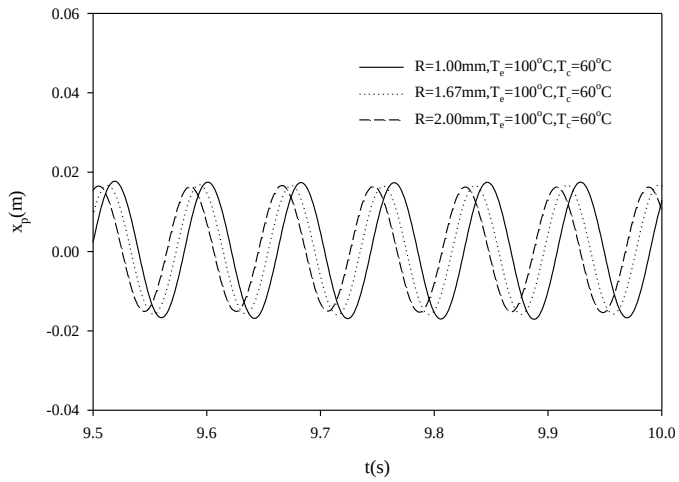

(a) Liquid slug displacement

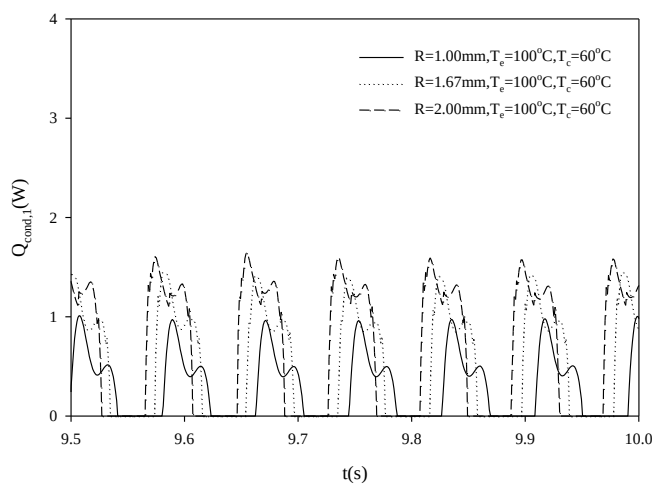

(b) Condensation heat transfer

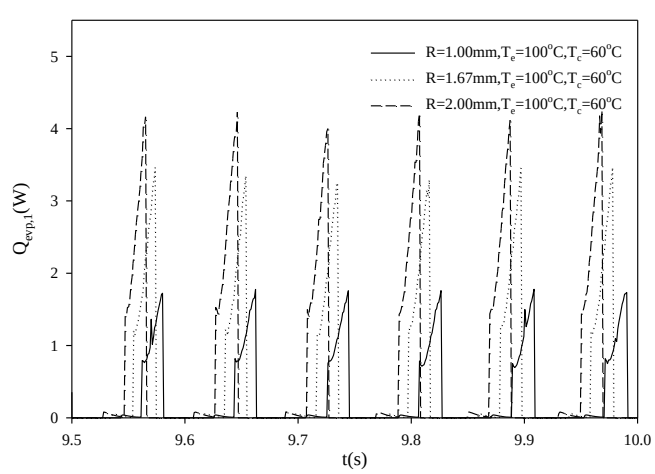

(c) Evaporation heat transfer

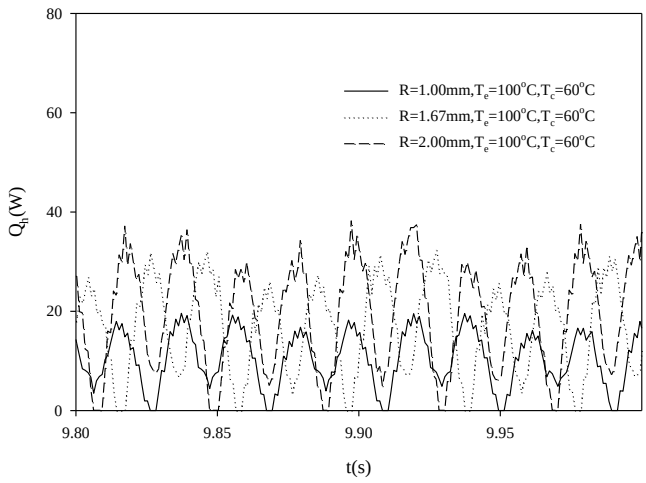

(d) Sensible heat transfer in

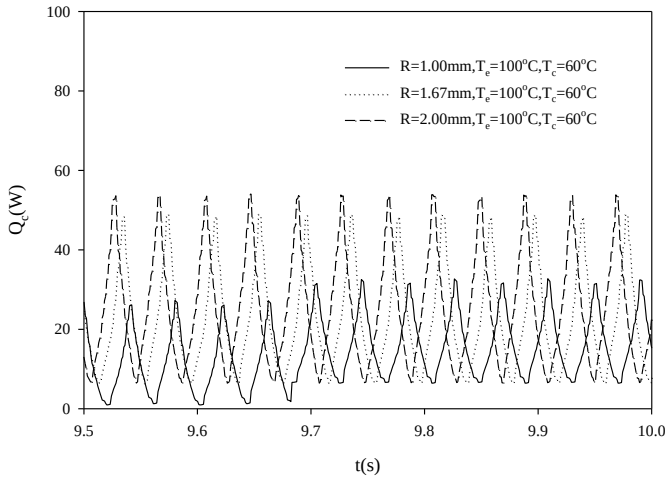

(e) Sensible heat transfer out

Figure 27 Influence of the inner diameter of the minichannel on the performance of the OHP

In Table 2, the heat transfer and oscillating flow performances under different operating conditions and assumptions are summarized. As can be seen, Case 7 has the highest sensible heat transfer rate and largest amplitude of the liquid slug oscillation. As the temperature difference between evaporator and condenser increase, the proportion of the latent heat transfer in total heat transfer decreases from 18.6% to 1.5%. When the evaporator temperature is decreased, both latent and sensible heat transfer are decreased. When the diameter decreases by half, the latent heat transfer decreases by half and the sensible heat transfer decreases by two thirds with a slowed down oscillation.

Table 2 Summary of heat transfer and fluid flow in a U-shaped minichannel

T_e (°C)	T_c (°C)	d (mm)	$\overline{Q_{evp}}$ (W)	$\overline{Q_{con}}$ (W)	$\overline{Q_h}$ (W)	$\overline{Q_c}$ (W)	$\overline{Q_t}$ (W)	$\frac{\overline{Q_l}}{\overline{Q_t}}$ (%)	$\frac{\overline{Q_s}}{\overline{Q_t}}$ (%)	Amplitude (m)	Period (s)
120°C	60°C	3.34	1.861	1.879	52.38	52.79	52.59	3.5	96.5	0.0217	0.077
110°C	60°C	3.34	1.478	1.458	33.01	34.06	33.54	4.4	95.6	0.0194	0.079
100 °C	60°C	3.34	1.055	1.065	16.7	23.0	20.95	5.0	95.0	0.0163	0.080
100°C	60°C	2.00	0.586	0.587	10.55	12.8	12.30	4.8	95.2	0.0171	0.082
100°C	60°C	4.00	1.303	1.321	19.29	25.4	23.65	5.5	95.5	0.0158	0.081
90°C	70°C	3.34	0.460	0.462	1.81	2.22	2.47	18.6	81.4	0.0086	0.081
100 °C	30°C	3.34	1.813	1.821	117.7	117.0	119.2	1.5	98.6	0.0295	0.091

4.4 Conclusion

Heat transfer models in the evaporator and condenser sections of an oscillating heat pipe are developed by analyzing thin-film evaporation and condensation, the effects of axial variation of surface temperature, the temperature of the evaporator and the inner diameter of the minichannel. The evaporation and condensation heat transfer coefficients are obtained by solving the thin film in the evaporator and thin film in the condenser and the test for those models shows that the models can produce a relative realistic latent heat transfer in a minichannel. The results confirmed that for all cases, heat transfer in an OHP is mainly due to the exchange of sensible heat. The effect of evaporator temperature on the oscillation and heat transfer is very significant. Decrease of the evaporator temperature decreases the total heat transfer rate and oscillating frequency and dampens the amplitude of the oscillation. The variation of the diameter of the minichannel has large impact on the heat transfer within the OHP while the oscillation is almost unaffected by the change of the tube diameter.

CHAPTER 5 CONCLUSIONS

5.1 Summary of This Work

The oscillatory flow of a U-shaped minchannel is simulated incorporating the pressure loss at the bend, surface tension, inclination angle and gravity. Heat transfer models in the evaporator and condenser sections of a U-shaped minichannel are developed by analyzing film evaporation and condensation and the effects of axial variation of surface temperature. The results confirmed that for all cases, heat transfer in an OHP is mainly due to the exchange of sensible heat. The effect of surface tension on the oscillation can be neglected. The gravitational force has more effect on the frequency of the oscillation than the amplitude. The bottom-heating mode operates most effectively. The effect of axial variation of surface temperature for laminar regime on the overall heat transfer is important. The effect of initial temperatures of working fluid on the oscillation and heat transfer is very significant. The evaporation and condensation heat transfer coefficients are obtained by solving the microfilm in the evaporator and condenser and the test for microfilm model shows that the models can produce a relative realistic latent heat transfer in a minichannel. The increase of the diameter of the minichannel has large impact on the heat transfer within the tube since both cross-sectional area and the area for heat transfer is significantly increased, while the oscillation is almost unaffected by the change of the tube diameter. The effect of pressure loss at the bend on the momentum equation of liquid slug is studied and the results show no remarkable effects on the flow

motion and heat transfer. Decrease of the evaporator temperature decreases the total heat transfer rate and oscillating frequency and dampens the amplitude of the oscillation.

5.2 Directions for Future Research

In this thesis as well as most of the existing models, the modeling of flow pattern transition is limited to one dimensional. In order to significantly advance the understanding of oscillatory flow and heat transfer in OHPs, the modeling of transient evaporation and condensation of thin film with more advanced techniques such as the volume of fluid (VOF) model to simulate 2-D/3-D two-phase flow and heat transfer will be helpful to obtain a more realistic description of transient flow and heat transfer in an OHP.

REFERENCES

[1] Akachi, H., "Looped Capillary Heat Pipes," Japanese Patent, No. Hei697147, 1994.

[2] Liang, S.B. and Ma, H.B., "Oscillating motions of slug flow in capillary tubes," International Comm. Heat and Mass Transfer, Vol.31, No. 3, 2004, pp. 365-375.

[3] Dobson, R.T., and Harms, T.M., "Lumped Parameter Analysis of Closed and Open Oscillatory Heat Pipe," Proceedings of the 11th International Heat Pipe Conference, Tokyo, Japan, 1999, pp. 137-142.

[4] Hosoda, M., Nishio, S., and Shirakashi, R., "Meandering closed-loop heat-transfer tube (propagation phenomena of vapor plug)," *Proceedings of the 5th ASME/JSME Joint Thermal Engineering Conference*, March 15–19, San Diego, CA, 1999.

[5] Wong, T.N., Tong, B.Y., Lim, S.M., Ooi, K.T., "Theoretical modeling of pulsating heat pipe," *Proceedings of the 11th International Heat Pipe Conference*, Tokyo, Japan, 1999, pp. 159-163.

[6] Zhang, Y., and Faghri, A., "Heat transfer in a pulsating heat pipe with open end," *International Journal of Heat and Mass Transfer*, Vol.45, No.18, 2002, pp. 2501-2508.

[7] Shafii, M.B., Faghri, A., and Zhang, Y., "Analysis of Heat transfer in Unlooped and Looped Pulsating Heat Pipes," *International Journal of Numerical Methods for Heat & Fluid Flow*, Vol. 12, No. 5, 2002, pp. 585 - 609.

[8] Zhang, Y., and Faghri, A., "Oscillating Flow in Pulsating Heat Pipes with Arbitrary Numbers of Turns," *AIAA Journal of Thermophysics and Heat Transfer*, Vol.17, No.3, 2003, pp.755-764

[9] Kiseev, V.M., and Zolkin, K.A., "The Influence of Acceleration on the Performance of Oscillating Heat Pipe", *Proceedings of 11th International Heat Pipe Conference*, Tokyo, Japan, 1999, pp. 154-158.

[10] Ma, H.B., Borgmeyer, B., Cheng, P., and Zhang, Y., "Heat Transport Capability in an Oscillating Heat Pipe," *Journal of Heat Transfer*, Vol. 130, 2008, pp. 081501.1-081501.7

[11] Khrustalev, D. and Faghri, A., "Thick-film phenomenon in high-heat-flux evaporation from cylindrical pores," *ASME Journal of heat transfer*, Vol.119, 1997, pp 272-278

[12] Begg, E., Khrustalev, D., and Faghri, A., "Complete condensation of forced convection two-phase flow in miniature tube," *ASME Journal of Heat Transfer*, Vol.121, 1999, pp. 904-915

[13] Kays, W.M., Crawford, M.E., and Weigand, B., *Convective Heat Transfer*, 4th ed., McGraw-Hill, New York, 1995, Chap. 8

[14] Gnielinski, V., "Neue Gleichungen für den Wärme- und den Stoffübergang in turbulent durchströmten Rohren und Kanälen," Forschung im Ingenieurwesen, Vol. 41, No. 1, 1975, pp. 8-16

[15] Rohsenow, W.M., Hartnett, J.P. and Ganic, E.N., *Handbook of Heat Transfer Fundamentals*, 2nd ed., McGraw-Hill, New York, 1985, Chap. 7

[16] Patankar, S.V., 1980, *Numerical Heat Transfer and Fluid Flow*, Hemisphere, New York, Chaps.2, 3

[17] Faghri, A., *Heat Pipe Science and Technology*, Taylor & Francis, Washington, DC, 1995

[18] Holm, F. W., and Goplen, S. P., "Heat Transfer in the Meniscus Thin-Film Transition Region," *ASME Journal of Heat Transfer*, Vol. 101, No. 3, 1979, pp. 543-547.

[19] Khrustalev, D, and Faghri, A., "Heat Transfer in the Inverted Meniscus Type Evaporator at High Heat Fluxes," *International Journal of Heat and Mass Transfer*, Vol. 38, No. 16,1995b, pp. 3091-3101.

[20] Cantrell, C. D., "Modern Mathematical Methods for Physicists and Engineers," *Journal of Measurement Science and Technology*, Vol. 12, No.12, 2001, pp. 702-712

PUBLICATIONS

[1] Shao, W., and Zhang, Y., "Thermally-Induced Oscillatory Flow and Heat Transfer in an Oscillating Heat Pip**e**," *Journal of Enhanced Heat Transfer* (in press), 2010

[2] Shao, W., and Zhang, Y., 2010, "Effects of Capillary Force and Gravity on Oscillatory Flow and Heat Transfer in an Oscillating Heat Pipe," *Proceedings of the 15th International Heat Pipe Conference*, 2010